Development of novel cytoprotective small compounds inhibiting mitochondria-dependent apoptosis

Mieko Matsuyama [1], Joseph T. Ortega [2], Yuri Fedorov [3], Jonah Scott-McKean [1, 4], Jeannie Muller-Greven [5], Matthias Buck [5], Drew Adams [3], Beata Jastrzebska [2], William Greenlee [6], Shigemi Matsuyama [1, 2, 7, 8, 9,10]

Department of Ophthalmology and Visual Science [1], Department of Pharmacology and Cleveland Center for Membrane and Structural Biology [2], Department of Genetics and Genome Science [3], Department of Macromolecular Science and Engineering [4], Department of Physiology and Biophysics [5], Department of Pathology [7],
Division of Hematology and Oncology. Department of Medicine [8],
School of Medicine [1,2,3,5,7,8], School of Engineering [4],
Case Western Reserve University
Case Comprehensive Cancer Center [9]
Harrington Discovery Institute [6]
Cleveland, OH
Corresponding author [10]

Running title: Novel Cell Death Inhibitor

Corresponding author: Shigemi Matsuyama, shigemi.matsuyama@case.edu

Keywords:
Bax, Apoptosis, Cell Death, Retinal Diseases, Photoreceptor,

Abstract

We identified cyto-protective small molecules (CSMs) by a cell-based high-throughput screening of Bax inhibitors. Through a medicinal chemistry program, M109S was developed, which is orally bioactive and penetrates the blood-brain/retina barriers. M109S protected retinal cells in the mouse models of Stargardt disease and macular degeneration. M109S directly interacted with Bax and inhibited the conformational change and mitochondrial translocation of Bax. M109S inhibited ABT-737-induced apoptosis both in Bax-only and Bak-only MEFs. M109S also inhibited apoptosis induced by staurosporine (mouse embryonic fibroblasts), etoposide (Neuro2a cells), and obatoclax (ARPE19 cells). M109S is a novel small molecule protecting cells from mitochondria-dependent apoptosis both *in vitro* and *in vivo*. M109S has the potential to become a new research tool for studying cell death mechanisms and to develop therapeutics targeting mitochondria-dependent cell death pathway. (128words)

39 **Introduction**

40 The Bcl-2 family of proteins is a group of evolutionarily conserved proteins regulating
41 mitochondria-dependent apoptosis (Reviewed in (Singh et al., 2019)). The abnormal balance of
42 these proteins induces apoptosis resistance of cancer cells and unwanted apoptosis of essential
43 cells in the damaged tissues(Singh *et al.*, 2019). Bax and Bak are the pro-apoptotic members of
44 the Bcl-2 family of proteins playing a central role in the mitochondria-dependent programmed
45 cell death (Wei et al., 2001). Since Bax/Bak double deficient cells are resistant to the stresses
46 activating the mitochondria-dependent apoptosis pathway (Wei *et al.*, 2001), Bax and Bak are
47 ideal pharmacological targets to control the life and death of the cells. The pharmacological
48 activators and inhibitors of Bax and Bak are expected to be effective in eliminating cancer cells
49 and rescuing essential cells from unwanted death, respectively (Diepstraten et al., 2022; Jensen et
50 al., 2019; Pogmore et al., 2021; Spitz and Gavathiotis, 2022; Walensky, 2019).

51 Previously, small compounds activating Bax/Bak-dependent apoptosis pathway have been
52 developed, and some of these small compounds are used clinically as effective therapeutics
53 eliminating cancer cells, for example, Venetoclax (Ashkenazi et al., 2017; Oltersdorf et al.,
54 2005). However, clinically effective small compounds rescuing damaged cells from Bax/Bak-
55 induced cell death have not yet been developed. Recent studies have reported the successful
56 development of Bax- inhibiting compounds (pro-drugs) by identifying small molecules inhibiting
57 the pore-forming activity (Niu et al., 2017) or the conformational change of Bax (Garner et al.,
58 2019). In addition, Elthrompag, an FDA-approved drug for thrombocytopenia, was found to
59 possess direct Bax binding and inhibiting activity (Spitz et al., 2021). These previous successes
60 were achieved by using an artificially reconstituted *in vitro* assay system. The compounds

61 identified by *in vitro* assay system will have the expected biochemical activity, however, there is
62 no guarantee that they will have the expected efficacy in living cells without unexpected toxic
63 effects. In this study, we utilized the cell-based functional screening system to develop novel
64 CSMs that rescue cells from Bax-induced apoptosis. The chemical structures of CSMs, described
65 here, are distinct from previously reported Bax inhibitors identified through the reconstituted *in*
66 *vitro* system. Through medicinal chemistry efforts, we succeeded in developing M109S which
67 has favorable pharmacokinetics in rodents. In this article, we report the chemical structures of
68 CSMs and their activities protecting cells at the levels of cell culture and mouse retinal disease
69 models.
70
71

72 ***Results***

73 **Development of cell-based Bax/Bak inhibitor screening system**

74 We generated cell lines that undergo apoptosis by the expression of Bax or Bak in

75 *bax*$^{-/-}$*bak*$^{-/-}$ mouse embryonic fibroblasts (MEFs). In these cells, the Tet-ON promoter (Loew et

76 al., 2010) is used for the induction of mCherry (red fluorescent protein), Bax, and Bak (Bax and

77 Bak are expressed without mCherry-tag). Therefore, expression levels of Bax and Bak can be

78 indirectly monitored by mCherry's red fluorescence intensity. These cells were named iRFP

79 (mCherry-inducible cells), iBax (Bax-inducible cells), or iBak (Bak-inducible cells) (Fig. 1A-C).

80

81 Doxycycline (Dox), a tetracycline analog, was used to activate the Tet-ON system, and the

82 expression of Bax and Bak was detected by Western blot at 6 h after the induction (Fig. 1B and

83 C). Forty-eight hours after the induction, many apoptotic cells can be observed by microscopic

84 analysis (Fig. 1D). To detect apoptotic nuclei, cells were stained with Hoechst dye (Fig. 1D).

85 These iBax cells were used to identify the candidates of CSMs. A 50,000 small compound

86 library was used to identify hit compounds by using a cell image analysis system (Operetta

87 system, Parkin-Elmer). The hits were selected by the following two criteria; 1) Decreasing the

88 percentages of dead cells detected (nuclear fragmentation and condensation), and 2) Maintaining

89 mCherry expression (fluorescence intensity) above 80% of the control so that compounds

90 inhibiting the Tet-ON system could be excluded. We then selected the top 50 compounds that

91 satisfied these criteria. Based on similarities in the chemical structure, the compounds were

92 divided into 2 groups. The best three small molecules rescuing iBax cells were M5, M6, and M7

93 (Fig. 1E). M5 and M6 (that have two enantiomers R and S) were assigned to Group 1, and M7 to

94 Group 2. Fig. 1D shows an example of M6S protecting iBax cells from Bax-induced apoptosis

95 while maintaining mCherry expression. These Bax-inhibiting hits were then tested in iBak cells.
96 However, none of these compounds were able to inhibit cell death induced by Bak in iBak cells
97 (Fig. 1D, example images of iBax and iBaK cells incubated with M6S 1 μM are shown). These
98 results suggest that CSMs can rescue cells from the apoptotic processes induced by the
99 overexpression of Bax but not Bak. The dose-response effects of M5, M5R, M5S, M6, M6R,
100 M6S, and M7 inhibiting Bax-induced apoptosis in iBax cells are shown in Fig. 1F. The S-
101 enantiomer showed a significantly higher cell death-inhibiting activity than the R-form in both
102 M5 and M6. Therefore, we focused on the S-enantiomer to perform Hit-to-Lead optimization in
103 Group 1. To be noted, the cell death inhibition activity of M5S is significantly higher than the
104 activities of Bax Channel Blocker(Bombrun et al., 2003) and iMac2 (Bombrun *et al.*, 2003;
105 Peixoto et al., 2009)(Fig.1G). Western blot analyses showed that these compounds did not
106 decrease Bax expression (Fig. 1H and I) but rather suppressed Caspase-3 activation (cleavage)
107 (Fig. 1H and L). The expression levels of endogenous Bax inhibitors such as Bcl-2 and Bcl-XL
108 did not show major changes (Fig. 1J and K).
109
110 **Hit-to-Lead optimization**
111 A medicinal chemistry program was carried out to expand the two lead series and optimize iBax
112 cell potency and Bax binding (explained later in Fig. 5E and G). A total of 200 new inhibitors
113 were designed and synthesized. Among them, M41S (Series 1) and M11 (Series 2) were the best
114 apoptosis inhibitors in iBax cells (Fig. 2A-C). The EC_{50} of M41S and M11 for the inhibition of
115 caspase activation in iBax cells were 3.8 nM (Fig. 2D) and 145 nM (Fig. 2C), respectively. In
116 comparison with the original hit compounds of M5 (S (EC_{50}=124 nM) and R (EC_{50}=1,450 nM)),
117 and M7 (EC_{50}=553 nM), apoptosis inhibiting activities of M41S and M11 were significantly

118 improved (Fig. 2B-D). Further optimization of the lead compounds (M41S) led to the
119 identification of the M109S lead compound protecting iBax cells with the EC_{50} of 23.4 nM (Fig.
120 2A and D). M109S exhibits drug-like profiles: Molecular Weight is 375, cLogP=4.0, kinetic
121 solubility is 0.05 uM in pH7.4 (clear suspension/solution can be prepared in 15% beta-
122 cyclodextrin solution at 2 mg M109S/ml), Caco-2 cell permeability is 11.7 x 10^{-6} cm/sec and the
123 efflux ratio is 1.3, microsomal stability (half-life (t ½)) is 46 min (human) or 11 min (mouse),
124 plasma protein binding is 99.97% (human) or 99.71 (mouse). The detail synthesis protocols and
125 pathways for M109S has been published (Matsuyama, 2020). As shown in Fig.2D, the apoptosis
126 inhibition activity of M41S and M109S in iBax cells is significantly higher than the activity of
127 Elthompag, a thrombopoietin receptor analog, which is recently reported to have Bax inhibitor
128 activity (Spitz *et al.*, 2021).
129

130 **M109 is an orally bioactive cell death inhibitor penetrating blood-brain/retina-barrier**

131 The pharmacokinetic (PK) analysis of M109S was performed in both mice and rats by oral gavage
132 (PO) and either by intraperitoneal (IP) or intravenous injection (IV) (Fig. 2E-G). In mice, M109S
133 reached 1.0 μg/ml (2.6 μM) plasma concentration within 30 min from administration, and it
134 remained at 596 ± 134 ng/ml (1.6 ± 0.36 μM) 24 h after the oral gavage administration (Fig. 2E).
135 Similar results were obtained in rats (Fig. 2F). At 24 h after the oral gavage administration, the
136 level of M109S in the plasma was 565.3 ± 188.3 nM in rats. Moreover, M109S crossed the blood-
137 brain and blood-retina barriers. The level of M109S in the rat retina and brain reached 171.0 ±
138 52.0 nM and 222.7 ± 74.7 nM, respectively, 24 h after its oral administration (Fig. 2F and G).
139 Notably, these concentrations are higher than the EC_{50} concentration (23.4 nM) of M109S

140 protecting iBax cells (Fig.2D). The half-life ($t_{1/2}$) of M109S (10 mg/kg body weight (b.w.) oral
141 administration) in the blood was longer than 12 h (in mice) or 9.7 h (in rats) (Fig. 2E and F).

142 **M109S protected the retina from the bright light-induced photoreceptor death**

143 Previous studies showed that Bax-mediated apoptosis plays an essential role in bright light-
144 induced retinal degeneration in *Abca4*$^{-/-}$*Rdh8*$^{-/-}$ mice(Sawada et al., 2014). *Abca4*$^{-/-}$*Rdh8*$^{-/-}$ mice
145 are mouse models of human Stargardt disease, a juvenile age-related macular degeneration (AMD)
146 that is susceptible to acute light insult and long-term retinal degeneration(Maeda et al., 2009)
147 (Sawada *et al.*, 2014) (Ortega et al., 2021). The retinal photoreceptor cells degenerate within 7
148 days in these mice after illumination with bright light due to apoptosis. An oral administration of
149 these mice with a total of four doses of M109S at 10 mg/kg b.w. within a scheme of two doses
150 before light exposure (24 h and 1h), followed by two doses after light exposure (24 h and 48 h),
151 produced protection of photoreceptor cells from death (Fig. 3A-H). The apoptotic processes
152 occurring in the photoreceptor cells upon bright light injury trigger the activation of an immune
153 response, which correlates with an increased number of autofluorescence (AF) spots in the retina.
154 The AF spots that can be detected with Scanning Laser Ophthalmoscopy (SLO) imaging represent
155 the activated resident microglia and peripheral immune cells that migrate to the retina to clear
156 dying photoreceptors. The increased number of AF spots was detected only in the vehicle-treated
157 mice. However, in mice treated with M109S at 10 mg/kg b.w., the number of AF spots was similar
158 to that detected in the dark-adapted mice (Fig. 3A, B, and S2). The loss of photoreceptors in the
159 vehicle-treated mice was evidenced by thinning of the outer nuclear cell layer (ONL) detected by
160 the optical coherence tomography (OCT), while the ONL in mice treated with M109S at 10 mg/kg
161 b.w closely reassembled the ONL in unexposed mice (Fig. 3C and D). While lower doses were
162 less effective (Fig. 3D and S3). The thickness of the ONL was confirmed by histological

163 examination of the H&E-stained retinal sections (Fig. 3E and G). Immunohistochemical staining
164 of rod and cone cells revealed healthy photoreceptors in mice pretreated with M109S prior to bright
165 light injury (Fig. 3F). The protection of the photoreceptor cells was confirmed in non-pigmented
166 WT Balb/cJ mice sensitive to light-induced retinal degeneration (Fig. 3H and S4). While exposure
167 to bright light triggered deterioration of photoreceptor cells in the vehicle-treated mice, oral
168 administration of M109S 24 h and 1 h prior to illumination followed by additional treatment 24 h
169 and 48 h after light exposure protected these mouse retinas. Altogether, these results indicate that
170 M109S protects retinal cells from bright light-induced death, and thus prevents retina degeneration
171 triggered by illumination.

172

173 **Evaluation of cell death inhibition activities of M109S in cultured cells.**

174 Next, we evaluated the effectiveness of M109S inhibition of cell death pharmacologically
175 induced in different cell types. ABT-737 is known to activate Bax/Bak-dependent apoptosis
176 pathway (Certo et al., 2006) (Vogler et al., 2009). The effects of M109S against ABT-737-
177 induced apoptosis were examined in MEF cells of wild type (*wt*) (Fig. 4A), $bax^{+/+}bak^{-/-}$ (Bax
178 only) (Fig. 4B), and $bax^{-/-}bak^{+/+}$ (Bak only) (Fig. 4C). M109S showed a dose-dependent
179 suppression of caspase activation in all three types of MEFs, suggesting that M109S can inhibit
180 apoptosis induced by Bax as well as Bak which are expressed at endogenous levels.
181 Staurosporine (STS), a pan-kinase inhibitor, is often used as a cytotoxic chemical activating
182 Bax/Bak-dependent mitochondria-induced apoptosis (Wei *et al.*, 2001). M109S inhibited
183 apoptosis induced by STS in MEFs (Fig. 4D). Etoposide, a topoisomerase inhibitor, is known to
184 activate DNA damage-induced cell death involving Bax/Bak-mediated apoptosis (Han et al.,
185 2019; Tu et al., 2009). M109S also significantly suppressed apoptosis induced by etoposide in

186 Neruo2a cells (Fig. 4E). However, in HeLa cells, M109S showed only slight inhibition (most of
187 the effects were not statistically significant) of etoposide-induced apoptosis (Fig. 4F and Fig.
188 S4), indicating that M109S inhibits etoposide-induced apoptosis in a cell type-dependent
189 manner. Obatoclax is known to induce both Bax/Bak-dependent and independent apoptosis in
190 certain types of cancer cells (Vogler *et al.*, 2009). M109S inhibited obatoclax-induced apoptosis
191 in ARPE19 cells (retina cell derived cancer cells). M109S suppressed caspase-3 activation
192 without a significant impact on Bax levels of obatoclax-treated ARPE19 cells (Fig. 4 G-I).
193

194 **M109S suppressed the conformation change (N-terminal exposure) and the mitochondrial**
195 **translocation of Bax**

196 The exposure of the N-terminus of Bax occurs as the early step of Bax-induced apoptosis (Hsu
197 and Youle, 1998; Nechushtan et al., 1999) . The levels of this conformational change can be
198 examined by immunoprecipitation of Bax by antibodies recognizing the N-terminus of Bax (Hsu
199 and Youle, 1998). As shown in Fig. 5A and B, CSMs (M41S, M11, and M109S) suppressed the
200 conformational change of Bax. Bax is known to translocate from the cytosol to the mitochondria
201 after the conformational change, which could be detected as higher density puncta in the DMSO-
202 treated control cells labeled with anti-Bax antibody (Fig. 5 C and D). (Nechushtan *et al.*, 1999).
203 CSMs (M41S, M11, and M109S) suppressed mitochondrial translocation of Bax in iBax cells
204 (Fig. 5 C and D).
205

206 **M019S directly binds to recombinant Bax protein**

207 We examined whether CSMs (M109S and M41S) directly bind Bax using a recombinant Bax
208 protein (Fig. 5E and S6). Binding was examined by the microscale thermophoresis (MST) assay

209 (Wienken et al., 2010). M109S showed Bax binding activity with the average Kd of 153.75±55.8
210 nM calculated from four independent MST assay results. Fig.5E shows an example of MST
211 assay detecting the biding of M109S and Bax (Kd=178nM). Dexamethasone is a steroid
212 hormone analog that has been shown to inhibit fibroblast cell death (Amsterdam et al., 2002;
213 Gascoyne et al., 2003), but it is not expected to bind Bax. Dexamethasone was used as a negative
214 control, and the binding of Dexamethasone and Bax was not detected (Fig. 5F).
215

216 **M109S decreases mitochondrial oxygen consumption and reactive oxygen species whereas**
217 **M109S increases glycolysis**

218 We noticed that the color of the culture medium of M109S-treated cells turned from red to
219 orange a little bit faster than that of vehicle control, suggesting that the medium acidification was
220 stimulated by M109S. Since lactate accumulation as the result of glycolysis is the common
221 reason for medium acidification in cell culture, we speculated that M109S has an activity
222 influencing cellular metabolism. To determine the effects of M109S on cellular metabolism,
223 oxygen consumption rate (OCR) and extracellular acidification rate (ECAR) were measured
224 using the Seahorse instrument. OCR and ECAR are the indicators of mitochondrial oxidative
225 phosphorylation (OXPHOS) and glycolysis, respectively. At 1 μM concentration in MEF cell
226 culture, M109S decreased maximal OCR and increased ECAR (Fig. 6A, C, E, and H).
227 Interestingly, similar effects were observed in *bax*$^{-/-}$*bak*$^{-/-}$ (Bax/Bak double knockout (DKO))
228 MEFs (Fig. 6B, D, F, and H), indicating that this activity on metabolism is independent of Bax
229 and Bak. Previous studies showed that OXPHOS inhibitors have neuroprotective activities by
230 decreasing reactive oxygen species (ROS) generation from mitochondria (Procaccio et al., 2014)
231 (Cunnane et al., 2020; Gao et al., 2021; Stojakovic et al., 2021). Therefore, the effects of M109S

232 on ROS were examined. As shown in Fig. 6I and J, M109S decreased ROS levels both in *wt* and
233 *bax*$^{-/-}$*bak*$^{-/-}$ DKO MEFs. N-acetyl cysteine (NAC) is known to reduce ROS levels in cells
234 (Ezerina et al., 2018). The effects of M109S (0.1- 1 μM) on the ROS level in cultured MEFs
235 were very similar to the effects of NAC (10-20 μM) (Fig.6I). Since the changes in the
236 metabolism can impact the speed of cell division, we examined the effects of M109S on
237 population doublings of cultured cells. M109S slightly decreased the speed of the population-
238 doubling time of cultured MEFs (Fig. 6K and L). The effect was more evident in *bax*$^{-/-}$*bak*$^{-/-}$
239 MEFs than in *wt* MEFs. Probably M109S's effects on cell division speed become more
240 detectable in *bax*$^{-/-}$*bak*$^{-/-}$ MEFs because the population doubling speed of *bax*$^{-/-}$*bak*$^{-/-}$ MEFs is
241 faster than that of *wt* MEFs. Altogether, these results indicate that independently of Bax
242 inhibiting effect, M109S also decreases the rate of oxygen consumption, which diminishes the
243 levels of ROS in the cell. These different activities of M109S have likely additive protective
244 effects against mitochondria-dependent cell death pathways.

245 ***Discussion***

246 We developed CSMs by utilizing a cell-based functional assay system that was developed to
247 identify Bax inhibitors. The chemical structures of these CSMs are distinct from previously
248 reported Bax inhibitors (Niu *et al.*, 2017) (Amgalan et al., 2020; Garner *et al.*, 2019; Spitz *et al.*,
249 2021) that were identified through *in vitro* Bax binding and pore-forming assays. Through a
250 medicinal chemistry program, M109S was developed as a lead compound which possesses cell
251 protecting activities both *in vitro* and *in vivo*. M109SS suppressed ABT-737-induced apoptosis
252 in both Bax-only and Bak-only MEFs (Fig. 4C). These observations suggest that M109S can
253 inhibit apoptosis induced by Bax and Bak expressed at endogenous levels in the cell. M109S also
254 inhibited apoptosis in STS-treated MEFs, obatoclax treated ARPE19 cells, and etoposide-treated
255 Neuro2a cells (Fig. 4 A-I). However, M109S did not inhibit etoposide-induced apoptosis in
256 HeLa cells (Fig. 4G), suggesting that M109S is not a universal cell death inhibitor. Etoposide
257 induces a certain level of cell death even in the absence of Bax and Bak (Han *et al.*, 2019; Tu *et*
258 *al.*, 2009). In the case of HeLa cells, Etoposide possibly activated the Bax/Bak-independent
259 pathway inducing apoptosis that cannot be inhibited by M109S. In the case of BAI-1, a
260 previously reported Bax inhibiting compound, it was reported that BAI-1 was not able to inhibit
261 Bax-induced apoptosis of the cancer cells due to the abnormally high levels of Bax expression in
262 the cancer cells(Amgalan *et al.*, 2020). Similar to BAI-1, M109S may show selective protection
263 against cell death depending on the expression levels of Bax and other apoptosis regulating
264 proteins.

265

266 M109S protected photoreceptor cells from the bright light-induced apoptosis in two mouse
267 models of light-induced retinal degeneration related to Stargardt's disease and age-related

268 macular degeneration (Maeda *et al.*, 2009) (Sawada *et al.*, 2014) (Ortega *et al.*, 2021). Previous
269 studies showed that Bax plays an essential role in photoreceptor death in these retina
270 degeneration mouse models(Maeda *et al.*, 2009) (Sawada *et al.*, 2014) (Ortega *et al.*, 2021). The
271 photoreceptor protection by M109S confirms that M109S penetrates the blood-retina barrier and
272 functions as Bax inhibitor *in vivo*. Indeed, M109S was detected in the brain and retina in rats 24
273 h after oral administration (Fig. 2G). Of note, no significant tolerability issues were detected in
274 the mice treated with M109S in these experiments. In addition, no significant off-target activities
275 were noticed at the concentration inhibiting apoptosis (EC50=23.4 nM) in Eurifine's 78
276 neurotoxicity tests (please see Supplemental Information of Eurifine Safety Scan test). Although
277 exploratory toxicity studies are planned, the currently available data suggest that M109S may
278 prevent the unwanted death of essential cells without significant side effects.
279
280 Bax biding activity of CSMs was confirmed by the MST binding assay. To be noted, the binding
281 of CSMs to Bax was detected in NP40-containing buffer but not in CHAPS-containing buffer
282 (Fig. S5). It is known that NP40, but not CHAPS, induces a conformation change (N-terminus
283 exposure) of Bax which is one of the activation steps of Bax(Hsu and Youle, 1998; Nechushtan
284 *et al.*, 1999). Therefore, the present data suggest that CSMs bind partially active Bax (the N-
285 terminus exposed Bax). The Bax binding character of CSMs is similar to that seen in anti-
286 apoptotic Bcl-2 family proteins such as Bcl-2 and Bcl-XL (Hsu and Youle, 1998; Nechushtan *et*
287 *al.*, 1999). For example, Bax binds Bcl-XL only in NP40-based buffer but not in CHAPS-
288 containing (or detergent-free) buffer if cell lysates were prepared from healthy cells (Hsu and
289 Youle, 1998). It is known that Bcl-XL, at the surface of the mitochondrial membrane, interacts
290 with activated Bax (the N-terminus exposed Bax) and bounces Bax back to the cytosol (Edlich

291 et al., 2011) (Todt et al., 2013). As a result, Bcl-XL suppresses the mitochondrial translocation of
292 Bax as well as the accumulation of active Bax in the cell, though the detailed mechanism of this
293 process is not yet understood. Similar to Bcl-XL, CSMs attenuated the N-terminus exposure of
294 Bax and suppressed mitochondrial translocation of Bax. CSMs and Bcl-XL may share a similar
295 mechanism of action to suppress Bax-induced cell death. Further biochemical and structural
296 biological studies are warranted to uncover the precise mechanism of action of Bax inhibition by
297 CSMs.
298
299 We found that M109S affects metabolism in 2 ways; 1) by decreasing mitochondrial oxygen
300 consumption and 2) by increasing glycolysis. It has been known that inhibitors of mitochondrial
301 oxidative phosphorylation (OXPHOS) have activities rescuing cells from mitochondria-
302 dependent cell death, especially in the case of ischemia/reperfusion-induced cell death (Gohil et
303 al., 2010; Morciano et al., 2018) (Hong and Pedersen, 2008) (Johnson and Ogbi, 2011) (Grover
304 and Malm, 2008) (Matsuyama et al., 1998). Furthermore, there is increasing evidence showing
305 OXPHOS inhibitors protect neurons in mouse models of neurodegenerative diseases including
306 Alzheimer's and Parkinson's diseases (Procaccio *et al.*, 2014) (Cunnane *et al.*, 2020; Gao *et al.*,
307 2021; Stojakovic *et al.*, 2021). These neuroprotective effects of OXPHOS inhibitors have been
308 explained by their activities decreasing ROS by suppressing mitochondrial oxygen consumption
309 (Procaccio *et al.*, 2014) (Cunnane *et al.*, 2020; Gao *et al.*, 2021; Stojakovic *et al.*, 2021). As
310 shown in Fig. 6, M109S decreased ROS in MEF cell culture. Therefore, in addition to the direct
311 inhibition of Bax, the suppression of mitochondrial activities may contribute to the cell
312 protection activity of M109S. However, these activities of M109S against mitochondrial
313 activities and metabolism became evident at 1 μM concentration in the cell culture (Fig.6) which

314 is approximately 40 times higher than M109S's EC50 (23.4 nM) of cell death inhibition (Fig.2).
315 Therefore, the effects on mitochondrial activity may become important only when M109S is
316 used at high dose.
317
318 In summary, we developed novel small compounds protecting cells from mitochondria-
319 dependent cell death. The pharmacokinetics of M109S is ideal for *in vivo* treatment. Importantly,
320 M109S reached both the brain and retina, indicating that M109S penetrates the blood-
321 brain/retina barrier. Bax-mediated and mitochondria-initiated cell death are involved in various
322 types of degenerative diseases including neurodegenerative disorders and cardiovascular
323 dysfunctions. M109S and its derivatives have the potential to become an important therapeutic
324 agent that can be used to prevent unwanted cell death in these pathological conditions. The
325 investigation of the mechanism of action of CSMs may shed new light on the previously
326 unknown cell death mechanisms controlled by Bax and Bak.
327
328 **Limitation of the study**
329 In the present study, we found that M109S prevented blindness of mouse models of Stargardt
330 disease and macular degeneration. However, these protective effects in mouse disease models do
331 not guarantee that M109S can prevent blindness in human and other animals. We plan to extend
332 our studies in other animals in the near future if fundings were obtained. In the present study, we
333 used a selected group pf cell lines (MEFs, Neruo2a, ARPE19, and HeLa cells) were used to
334 investigate the mechanism of cell death inhibition by M109S. It is not yet certain whether the
335 similar results can be seen in other cell lines. We plan to examine other types of primary cultured
336 cells and cancer cell lines to further investigate the mechanism of action of M109S.
337

338 **KEY RESOURCE TABLE**

339

REAGENT or RESOURCE	SOURCE	IDENTIFIER
Antibodies		
anti-Bax polyclonal antibody	ProteinTech	50599-2-IG
anti-Bax Rabbit Polyclonal antibody	BD Pharmingen	BD 554104
Agarose beads conjugated with anti-Bax monoclonal antibody (clone 6A7)	Santa Cruz	sc-23959AC
anti-Bak	Santa Cruz	sc-832
anti-Bcl-XL	Santa Cruz	sc-1690
anti-Caspase-3	Cell Signaling	9662s
anti-beta actin	Sigma-Aldrich	A5441
Anti-rabbit IgG-HRP	Kindle Bioscience	R1006
Anti-mouse IgG-HRP	Kindle Bioscience	R1005
Goat-anti-Mouse IgG (H+L)	Life Tech	G-21040
Culture medium		
DMEM	ThermoFisher	11995
Fetal Calf Serum	Fisher Scientific	12999102
Doxycycline Hyclate	SigmaAldrich	33429-100MG-R
Puromycin	Dot scientific	DSP33020-0.025
Geneticin (G418)	ThermoFisher Scientific	10131027
Penicillin/Streptomycin	Fisher	SV30010
Chemicals, peptides, and recombinant proteins		
(2-Hydroxypropyl)-beta-cyclodexitrin (bCD)	Sigma-Aldrich	332607
Etoposide	Sigma-Aldrich	E1383
ABT-737	Sellekchem	S1002
Obatoclax	Cayman Chemical	11499
Staurosporine	Sigma-Aldrich	No. S6942
Dexamethasone	Sigma-Aldrich	D4902
M5 (R, S)	This study	
M6 (R, S)	This study	
M7 (R, S)	This study	
M11	This study	
M109S	This study	
Bax Channle Blocker	Tocris	No. 2160
iMac2	Tocris	No. 3749
Elthrompag	Sigma-Aldrich	SML3182
Critical commercial assays		
Capsase-Glo 3/7 Assay kit	Promega	G8093
ROS-Glo-H_2O_2 Assay kit	Promega	G8820
His-Tag labeling Kit RED-tris-NTA 2nd generation	Nanotemper	MO-L018
XF Cell Mito Stress test kit	Agilent	103015-100

Deposited data		
NA		
Experimental models: Cell lines		
iWT (wild type MEF, C57BL6 from The Jackson Lab)	This study	
iBBKO (Bax Bak doublr KO MEFs	This study	
iRFP (mCherry inducible iBBKO)	This study	
iBax (Bax inducible iBBKO)	This study	
iBak (Bak inducible iBBKO)	This study	
HeLa	ATCC	CRM-CCL-2
Neuro2a	ATCC	CCL-131
ARPE19	ATCC	CRL-2302
Experimental models: Organisms/strains		
Balb/c mouse	Jackson Lab	000651
Abc4-/-Rdh8-/- mouse	Jackson Lab	030503
Recombinant DNA		
pLVX-EF1a-TET3G	Takarabio	631359
pLVX-TRE3G-mCehrry	Takarabio	631360
Software and algorithms		
Prism	Dotmatics Graphpad	https://www.graphpad.com/scientific-software/prism/

340

341
342 # STAR Methods
343

344 ## RESOURCE AVAILABILITY

345 ### Lead contact

346 Further information and requests for resources and reagents should be directed to and will be
347 fulfilled by the lead contact, Shigemi Matsuyama (shigemi.matsuyama@case.edu).

348

349 ### Materials availability

350 There are restrictions on the availability of all newly synthesized chemicals and cell lines used in
351 this study due to potential requirements for materials transfer agreements with the host institution
352 where these materials were generated.

353

354 ### Data and code availability

355 Any additional information required to reanalyze the data reported in this paper is available upon
356 request from the lead contact.

357

358 ## METHOD DETAILS

359

360 ### Cell Culture and Generation of iRFP, iBax, and iBak Cells

361 Mouse embryonic fibroblasts (MEFs) from *wt* and *bax*$^{-/-}$*bak*$^{-/-}$ mice (C57BL/6J background,
362 generated by crossing *bax*$^{+/-}$ and *bak*$^{-/-}$ mice originally obtained from The Jackson Lab) were
363 established in Matsuyama lab, and were immortalized by SV40LT expression. To introduce Tet-
364 ON system (Tets-On inducible system, Takara, Madison, WI), a set of two plasmids were

365 introduced to *bax*$^{-/-}$*bak*$^{-/-}$ MEFs to establish each cell line. The pLVX-EF1a-TET3G carrying Tet-
366 inducible transcription factor was used for all three cell lines. pLVX-TRE3G-mCehrry (original
367 plasmid with only mCherry), pLVX -TRE3G-mCherry carrying cDNAs of human Bax or human
368 Bak, were introduced to generate cell lines of iRFP, iBax, and iBak respectively. These plasmids
369 were introduced into the cells by using Lentivirus transfection system. Doxycycline (Dox) (100
370 ng/ml) was used to activate Tet-ON system to induce mCherry, Bax, and Bak. To maintain
371 transfected genes, puromycin (1 ug/ml) sand G418 (750 ug/ml) were added to the MEF medium.
372 The MEF medium is made from DMEM High Glucose (ThermoFisher Catlog Number11995)
373 supplemented with 10% Fetal Calf Serum (FCS, Fisger Scientific Cat No.12999102), 2 mM
374 (final concentration) Sodium Pyruvate, 6 mM L-Glutamine (Final concentration), 100U/ml
375 (Penicillin-Streptomycin), and 1% of Non-Essential Amino Acid supplement (Gibco, 11140-
376 050).
377
378 **High-Throughput Screening of Small Compound Library**
379 We used a 50,000 small compound library purchased from ChemBridge (San Diego, CA) to
380 identify the compounds protecting cells from Bax-induced cell death using iBax cells (passage
381 of iBax cells were used in the screening). 386 well plates and Operetta Image analysis system
382 (Perkin Elmer) were used for the screening. First, each compound was added together with Dox
383 (100 ng/ml) to the culture media of iBax cells to the final concentration of 10 μM. Cells were
384 cultured for 48 h and fixed by 2% paraformaldehyde (PFA) and the nuclei were stained with
385 Hoechst 33258. Cell images were captured using both RFP and DAPI filter channels. RFP filter
386 channel was used to monitor the mCherry expression. The compounds maintaining 80% and
387 higher mCherry expression of the control cells (only Dox addition) were analyzed. DAPI filter

388 channel was used to analyze the percentage (%) of cells with apoptotic nuclei (pyknosis). The
389 best 50 chemicals were selected, and they were subjected to examine the dose-dependent effects
390 to confirm the cytoprotective activities. After the best 50 hit compounds were selected, and two
391 groups of chemicals were found Group 1 (M5 and M6 were the best Bax inhibitors in this group)
392 and Group 2 (M7 was the best Bax inhibitor in this group)). We examined whether these 50
393 chemicals can also inhibit Bak-induced cell death in iBak cells. However, these compounds were
394 not effective in inhibiting Bak-induced cell death in iBak cells.
395
396 **Chemical Synthesis and profiling tests**
397 All the chemical synthesis were performed by Wuxi AppTech (Hong-Kong, China) based on the
398 chemical design by Dr. William Greenlee. To select the lead compounds, the hit compounds
399 were subjected to the profiling tests examining, kinetic solubility, Caco-2 cell, microsomal
400 stability (t ½ min), and plasma protein binding.
401
402 **Western Blot**
403 To analyze the expression levels of Bcl-2 family proteins, Caspase-3, and beta-tubulin, cells
404 were lysed in RIPA buffer and 20 micro-g of total protein was subjected to Western blot analysis
405 using 4-20% gradient gel (Invitrogen). The primary antibodies used in this study are: anti-Bax
406 antibody (Proteintech, 50599-2-IG, 5000X), anti-Bcl-2 antibody (SantaCruz, sc-7382, 500X),
407 anti-Bc-XL antibody (SantaCruz, sc-1690, 500X), Caspase-3 (Cell Signaling, 9662, 1000X), and
408 anti-beta actin (Sigma Aldrich, A5441, 20,000X). The secondary antibodies used for this study
409 were anti-Rabbit-HRP (Kindle Biosciences, R1006, 1000X) and anti-mouse IgG-HRP (Kindle

410 Biosciences, R1005, 1000X). Western blot signals were captured by Kwik Quant Imager (Kindle
411 Biosciences), and the densitometric analysis was performed by Image J.
412
413 **Caspase Measurement**
414 Promega's Capsase-Glo 3/7 Assay kit (G8093, Promega) was used to measure caspase activity
415 according to the manufacturer's protocol. iBax and MEFs (ABT-737- and Staurosporine (STS)-
416 induced apoptosis): iBax cells or MEFs were seeded at the density of 16,000 cells/100 μl/well
417 (for ABT-737) or 20,000 cells/100 μl/well (for STS) in 96 well plates on Day 0. For culture
418 medium, MEF medium was used (please see "Cell Culture" section). To determine the effects of
419 CSMs on Caspase activation by Bax overexpression, Dox (100 ng/ml) and CSMs (various
420 concentrations as indicated in the figures) were added to the culture media on Day 1. On Day 3,
421 cells were subjected to Caspase assay. To examine the effects of CSMs against 1 μM ABT-737
422 (S1002, Sellekchem), cells were treated with ABT-737 together with various concentrations of
423 CSMs. On Day 1 (*wt* (passage 10) and Bax only (passage 11) cells) and Day 2 (Bak only cells
424 (passage 10), Bak only cells die slower than wt and Bax-only cells)), Caspase activity was
425 measured. To examine the effects of M109S against STS-induced apoptosis, MEFs were pre-
426 incubated with M109S for 2 h before STS (1 μM) addition to the medium. Four hours after STS
427 addition, Caspase assay buffer containing cell lysis reagent was added to each well, and cells
428 were subjected to Caspase measurement. Neuro2a and HeLa cells (Etoposide-induced apoptosis:
429 Cells were seeded at the density of 10,000 cells/100 μl/well in 96 well plates on Day 0. On day
430 1, etoposide (25 μM to Neuro2a (ATCC, passage 12), 12.5 or 25.0 μM or HeLa cells (ATCC,
431 passage 11), respectively) were added to the culture media. On day 2, media were replaced with

432 fresh media containing various concentrations of M109S without etoposide. On day 3, Caspase
433 assay buffer was added to each well and Caspase activity was measured.
434
435 **Pharmacokinetic Analysis**
436 The compounds were dissolved in 15% (2-Hydroxypropyl)-beta-cyclodexitrin (bCD) (and they
437 were administered to the mice or rats by oral gavage, intrapreneurial (i.p.), or intravenous (i.v.)
438 injection. At the time point of 0.5, 1, 2, 4, 8, and 24 h, the concentration in the blood plasma (3
439 mice for each time point) were measured by Mass Spectrometry analysis. The concentrations in
440 the retina and brain were also measured 24 h after the administration. These PK analyses of mice
441 and rats were performed by Wuxi AppTech (Hong-Kong, China) and PharmOptima (Portage,
442 Michigan).
443
444 **Animals Care and Treatment.** Double knockout mice *Abca4*$^{-/-}$*Rdh8*$^{-/-}$ with 129Sv or C57BL/6
445 background that lacks ABCA4 transporter and retinol dehydrogenase 8 (RDH8) (Maeda et al.,
446 2008) at 5–6 weeks of age were used to evaluate the protective effect of a novel BAX inhibitor
447 (M109S) on retinal degeneration induced by acute light. *Abca4*$^{-/-}$*Rdh8*$^{-/-}$ mice do not carry the
448 *Rd8* mutation, however, they carry the Leu variation at amino acid 450 of retinal pigment
449 epithelium 65 kDa protein (RPE65) (Gao et al., 2018; Kim et al., 2004). The substitution of Leu
450 to Met in the *Rpe65* gene that exists in inbreed mice decreases sensitivity to retinal damage induced
451 by bright light (Kim *et al.*, 2004). Balb/cJ (RRID:IMSR_JAX:000651) mice were used as WT
452 control. Both male and female mice were used in all experiments. All mice were housed in the
453 Animal Resource Center at the School of Medicine, Case Western Reserve University (CWRU),
454 and maintained in a 12-hour light/dark cycle. All animal procedures and experimental protocols

455 were approved by the Institutional Animal Care and Use Committee at CWRU and conformed to
456 recommendations of both the American Veterinary Medical Association Panel on Euthanasia and
457 the Association for Research in Vision and Ophthalmology.

458

459 **Retinal Degeneration Induced with Bright Light.** Twenty four hours before the treatment 4-5
460 weeks old *Abca4*$^{-/-}$*Rdh8*$^{-/-}$ mice and 6-8 weeks old Balb/cJ mice were dark-adapted. M109 was
461 dissolved in the 2-hydroxypropyl-β-cyclodextrin vehicle and administered to mice by gavage.
462 *Abca4*$^{-/-}$*Rdh8*$^{-/-}$ mice were administered with M109S at 1, 2.5, 5, 10, and 20 mg/kg body weight
463 (b.w.) 24 h and 2 h before the exposure to light, while Balb/cJ mice were gavaged with M109S at
464 a dose of 20 mg/kg b.w. 2-hydroxypropyl-β-cyclodextrin vehicle was administered to control mice.
465 To initiate the retinal damage, mice pupils were dilated with 1% tropicamide and *Abca4*$^{-/-}$*Rdh8*$^{-/-}$
466 mice were exposed to 10,000 lux white light for 30 min, delivered from a 150-W bulb (Hampton
467 Bay; Home Depot, Atlanta, GA) (Chen et al., 2012). Balb/cJ mice were exposed to 12,000 lux
468 light for 2 h. After illumination, mice were kept in the dark for 7 days. Treatment with M109 or
469 vehicle was repeated 24 and 48 h after the exposure to light. The health of the retina was assessed
470 *in vivo* by imaging using spectral domain optical coherence tomography (SD-OCT). Next, mice
471 were euthanized and eyes were collected for histological evaluation. Six mice were used in each
472 experimental group.

473

474 **SLO.** The Scanning Laser Ophthalmoscopy (SLO) (Heidelberg Engineering, Franklin, MA) was
475 used to image the *in vivo* whole-fundus mouse retinas. *Abca4*$^{-/-}$*Rdh8*$^{-/-}$ mice were subjected to
476 SLO imaging immediately after the acquired SD-OCT imaging. The number of autofluorescent

477 spots (AF) detected in different experimental groups was quantified and compared to determine
478 the statistical significance. Six mice were used in each experimental group.

479

480 **SD-OCT.** Ultrahigh-resolution SD-OCT (Bioptigen, Morrisville, NC) *in vivo* imaging was used
481 to evaluate the effect of M109S treatment on retinal structure in *Abca4*$^{-/-}$*Rdh8*$^{-/-}$ mice subjected
482 to bright light-induced retinal damage (Chen *et al.*, 2012). Before imaging, mice pupils were
483 dilated with 1% tropicamide and anesthetized by i.p. injection of a cocktail containing ketamine
484 (20 mg/ml) and xylazine (1.75 mg/ml) at a dose of 4 µl/g b.w. The a-scan/b-scan ratio was set at
485 1200 lines. The retinal images were obtained by scanning at 0 and 90 degrees in the b-mode. Five
486 image frames were captured and averaged. To determine the changes in the retinas of mice treated
487 with M109S and exposed to bright light and control mice treated with vehicle or non-treated and
488 dark-adapted mice were determined by measuring the outer nuclear layer (ONL) thickness at 0.15-
489 0.75 mm from the optic nerve head (ONH). Values of the ONL thickness were plotted using means
490 and standard deviation. For each experimental group, six mice were used.

491

492 **Retinal Histology.** The effect of M109S on the retinal morphology in *Abca4*$^{-/-}$*Rdh8*$^{-/-}$ mice
493 exposed to bright light was determined by retinal histology analysis. Eyes were collected from
494 non-treated mice kept in the dark, treated with 2-hydroxypropyl-β-cyclodextrin vehicle or M109S,
495 and illuminated with bright light. Eyes were collected from euthanized mice and fixed in 10%
496 formalin in PBS for 24 h at room temperature (RT) on a rocking platform, followed by paraffin
497 sectioning. Sections (5 µm thick) were stained with hematoxylin and eosin (H&E) and imaged by
498 a BX60 upright microscope (Olympus, Tokyo, Japan). Then, the data were processed using

499 MetaMorph software (Molecular Devices, Sunnyvale, CA, USA). Six mice were used in each
500 experimental group.

501

502 **Immunohistochemical Analysis.** To detect the rod and cone photoreceptors in the retina, eyes
503 were collected from euthanized *Abca4*$^{-/-}$*Rdh8*$^{-/-}$ mice one week after the treatment and fixed in
504 4% PFA for 24 h followed by their incubation in 1% PFA for 48 h at RT. The eight-µm thick
505 cryosections prepared from fixed eyes were incubated at 37°C for 10 min, followed by hydration
506 with PBS for 2 min. These sections were blocked with 10% normal goat serum (NGS) and 0.3%
507 Triton X-100 in PBS for 1 h at room temperature. Then sections were stained with a mouse 1D4
508 anti-rhodopsin primary antibody to visualize rods and biotinylated peanut agglutinin (PNA) (1:500
509 dilution) to visualize cones overnight at 4°C. The next day, sections were washed with PBS,
510 followed by the incubation with Alexa Fluor 555-conjugated goat anti-mouse secondary antibody
511 (1:400 dilution) to detect rods and Fluor 488-conjugated streptavidin (1:500 dilution) to detect
512 cones for 2.5 h at room temperature. Cell nuclei were stained with DAPI. Slides were coverslipped
513 with Fluoromount-G (SouthernBiotech). The retina was imaged with the Olympus FV1200 Laser
514 Scanning Microscope (Olympus America, Waltham, MA) and 40x/1.4 objective.

515

516 **6A7 Ab Bax Immunoprecipitation**

517 Immunoprecipitation of activated Bax (The N-terminus exposed Bax) was performed as
518 previously reported (Gama et al., 2009). Cell lysates were prepared with 1% CHAPS buffer. The
519 cell lysates of 150 ul (5 mg/ml protein concentration) were incubated with 10 ul of 6A7
520 antibody-conjugated agarose beads (sc-23959AC, Santa Cruze) at 4C for 2 hrs. Then, the beads
521 were washed with the CHAPS buffer 3 times, and the immunoprecipitated Bax was eluted by

522 incubating the beads with 50 ul of Lamili buffer at 95C for 10 min. Fifteen (15) ul of the eluted
523 samples was subjected to Western blot. For the detection of the total Bax expression in the cell
524 lysate, 20 μg of total protein was subjected for each lane of the gel. To detect Bax in Western
525 blot, an anti-Bax polyclonal antibody (50599-2-IG, Protein Tech) was used.
526
527 **Bax Immunocytochemistry**
528 On Day 0, iBax cells (15,000 cells/100 μl/well) were seeded in 96 well plates, On Day 1, Dox
529 (100 ng/ml) was added together with CSMs. After 36 h of Dox addition, cells were fixed by 2%
530 PFA and subjected to immunocytochemistry. Anti-Bax polyclonal antibody (50599-2-IG, Protein
531 Tech) was used to detect Bax in the cells. The pictures of Bax staining (green fluorescence),
532 mCherry expression (red fluorescence), and normal light image were taken and used to
533 determine the percentages of cells showing punctuated Bax staining among Bax expressing cells.
534 At least 200 cells were counted from each image. At least 3 wells were used for each condition.
535
536 **Microscale Thermophoresis (MST)**
537 His-Tag labeling Kit RED-tris-NTA 2nd generation (MO-L018, Nanotemper) was used to label
538 His-tagged Bax purchased from Creative BioMart (Catalog No. BAX-6976H, Seattle, WA). His-
539 Bax (210 μl/ml in Phosphate Buffer Saline (PBS) (pH7.4)) was aliquoted (10 μl/tube) and kept at
540 -80C. For RED labeling, 0.05% CHAPS PBS was used to dissolve the RED dye. The final
541 concentration of the labeled Bax protein was 50 nM for the binding assay and was mixed with a
542 serial dilution of CSMs. The first concentration of CSMs (20 μM) was prepared in PBS with 1%
543 BSA and 2% NP40. The final condition of the buffer for binding was PBS with 0.5% BSA and
544 1% NP40 in all 16 reaction tubes. When 1% NP40 was replaced with 1% CHAPS, the dose-

545 dependent binding signal was not detected as explained in Discussion. The labeled His-Bax was
546 kept on ice and used within 3 hrs after the labeling. The measurement of dissociation constant
547 Kd was performed by the NanoTemper's software installed in the Monolith system.
548
549 **Seahorse Experiment**
550 XF Cell Mito Stress test kit (103015-100) was used to measure OCR and ECAR with the XFe96
551 Seahorse instrument. On Day 0, the cell culture of MEFs was started ($1.6x10^4$ cells/200 micro-
552 l/well (Agilent, XF96 microplate V3-PS)) using a MEF medium. On Day 1, CSMs were added to
553 the culture medium (10 nM, 100nM, or 1 μM) and incubated for 4 hrs in a CO_2 incubator. After
554 the incubation, the medium was changed with XF DMEM medium (Agilent, 103575-100), and
555 cells were incubated in a 37 ºC chamber (100% air) for 1 hr before the mitochondria stress test.
556 For the test, rotenone (0.5 μM), antimycin A (0.5 μM), oligomycin (1.5 μM), and FCCP (2.0
557 μM) were used according to the manufacturer's protocol. OCR and ECAR were recorded and the
558 effects of CSMs on OXPHOS and glycolysis were analyzed.
559
560 **ROS Measurement**
561 ROS-Glo-H_2O_2 Assay kit (Promega G8820) was used to measure ROS in MEFs culture (medium
562 and cells) according to the manufacturer's protocol. On day 0, cells were seeded at the
563 concentration of 16,000 cells/100 μl/well in 96-well plate. On day 1 (24 hr after the start of cell
564 culture), cells were pre-incubated with DMSO only (Control) (0.001%) or M109S (100 nM, 200
565 nM, 1 μM (the final DMSO was adjusted to 0.001% in all the conditions) for 4 hrs. Then, the
566 medium was changed to a new medium containing 25 μM H2O2 substrate with DMSO or
567 M109S (medium in each well was 100 μl). Cells were cultured in a CO_2 incubator for additional

568 4 hrs. Then, 100 µl of ROS-glo Detection solution was added to each well and incubated for 20
569 min at room temperature. Luminescence intensity from each well was recorded by MG3500
570 (Promega) plate reader.
571
572 **Cell Number Measurement**
573 On Day 0, the cell culture of MEFs was seeded ($4x10^5$ cells/ml/well (12 well plate)). On day 1,
574 24 hrs after the starting of the cell culture, the various concentration of CSMs were added to the
575 culture medium. On Day 2, 48 hrs after the start, cells were collected, and cell number was
576 counted by an automated cell counter (Countess II, Invitrogen). Four wells were used for one
577 condition.
578
579 **Statistical Analysis**
580 For Fig.1, 2, 4, 5, and 6, Statistical analyses and calculations of EC_{50} were performed using
581 Prism (version 9.4.1). Student's t-test was used to determine the statistical significance in *in vitro*
582 experiments. For Fig.3: The statistical analysis of treatment with M109S in mouse models one or
583 two-way ANOVA with Turkey's post hoc tests were used. All statistical calculations were
584 performed using the Prism GraphPad 7.02 software. Type 1 error tolerance for the experiments
585 was assumed at 5%. Values of $P < 0.05$ were considered statistically significant. Data collection
586 and statistical analysis were performed by different personnel.
587

588 **Author Contribution**

589

590 Shigemi Matsuyama initiated the project and designed the experiments reported in Fig. 1, 2, 4,
591 and 5. iRFP cells, iBax cells, and iBak cells as well as the CSM screening system were designed
592 and generated by Shigemi Matsuyama. Mieko Matsuyama performed the experiments together
593 with Shigemi Matsuyama reported in Fig. 1, 2 (except Fig. 2 E-G), 4, and 5. Jonah Scott-
594 McKean analyzed the data of Fig. 1F. Joseph Ortega and Beata Jastrzebska designed and
595 performed the experiments reported in Fig. 3. Yuri Fedorov and Drew Adams set up the high-
596 throughput drug screening system with the Operetta system (Parkin Elmer), optimized the CSM
597 screening system, and performed the screening. Jeannie Muller-Greven and Mathias Buck
598 provide advice for the MST-binding assay and participated in the data analysis. William
599 Greenlee performed the medicinal chemistry study during the entire project, and he designed all
600 the novel CSMs. The first draft of the manuscript was prepared by Shigemi Matsuyama, and all
601 the authors participated in editing the draft to complete the final version.

602

603

Acknowledgement

Authors are grateful for invaluable advice and guidance by Dr. Diana Wetmore (HDI) and Dr. Steven Brenner (HDI) throughout the project, and for project management by Dr. Jeff Klein (HDI). We thank the past and present members of Matsuyama laboratory (Dr. James Palmer, Dr. Kelsey Jensen, David J WuWong, Sean Wang, Emma Heironimus, and Xiao-Yi Chen) for their assistance in plasmid production, cell image capture, and data analysis. We also thank Dr. David Wald for his advice on drug screening and the use of the Tet-ON system. This work was supported by Gund-Harrington Scholar Award (to SM) from Foundation Fighting Blindness and Harrington Discovery Institute (HDI), Department of Defense Vision Research Program W81XWH-20-1-0735 (to SM), National Institute of Health (NIH) RO1-AG031903 (to SM), RO1 EY032874 (to BJ), RO1EY029169 (JMG and MB), P30 grants for Case Comprehensive Cancer Center and Vision Science Research Center.

619 **Figure 1. Development of Bax- or Bak-inducible system in *bax*$^{-/-}$*bak*$^{-/-}$ MEFs and the**
620 **screening of small compounds rescuing cells from Bax or Bak.**
621
622 A: Doxocyclin (Dox)-induced expression of Bax and Bak in MEFs. Dox-inducible Bax or Bak
623 (no-tag) gene was introduced in *bax*$^{-/-}$*bak*$^{-/-}$ MEFs by Lentivirus vectors. These cells were named
624 iBax or iBak cells, respectively. The cells expressing only mCherry was named iRFP cells.
625
626 B and C: Western blot analysis of the expression levels of Bax or Bak in wild-type (*wt*) MEFs,
627 iBax, iBak cells are shown (B). The results of densitometric analyses are shown in C. The
628 expression levels of Bax and Bak in *wt* MEFs were designated as 1 (actin levels were used as
629 loading control). The error bars indicate SD. The result of the t-test statistical analysis is shown.
630 Statistically significant difference ($p<0.05$) is indicated in the figure.
631
632 D: Cell images of iRFP, iBax, and iBak. The Dox-inducible mCherry (red fluorescent protein)
633 gene was introduced in *bax*$^{-/-}$*bak*$^{-/-}$ to monitor Dox-inducible gene expression. Pictures were
634 taken 48 h after Dox addition (100 ng/ml) to the medium. Images show cells under normal light,
635 stained with Hoechst dye (nuclear staining), and expressing mCherry. Cell death (nuclear
636 condensation and fragmentation), as well as apoptotic bodies (mCherry images), can be observed
637 in these images. M6S is one of the hit compounds suppressing Bax-induced cell death. M6S (1
638 μM) rescued iBax cells, but not iBak cells.
639
640 E: Chemical structures of hit compounds are shown.
641

642 F: The dose-dependent inhibition of Bax-induced apoptosis in iBax cells by M5, M6, and M7
643 that were the best three representative hit compounds. The % of apoptosis was measured by the
644 detection of apoptotic nuclei by Hoechst dye nuclear staining. The enantiomer S form of M5 and
645 M6 (M5S and M6S) showed significantly stronger activities than the enantiomer R form (M5R
646 and M6R). The original compounds in the library (M5 and M6) were a mixture of S and R forms
647 with unknown ratio.
648
649 G: The dose-dependent effects of M5S, iMac2, and Bax Channel Blocker suppressing cell death
650 in iBax system is shown. M5S showed significantly stronger activity to inhibit cell death in iBax
651 cells.
652
653 H-L: Western blot analysis of Bcl-2 family proteins and Caspase-3 in iBax cells treated with M5,
654 M6, and M7. iBax cells were incubated for 48 h with or without Dox (100 ng/ml) in the presence
655 or absence of M5, M6, or M7. M5 and M6 are the original hit compounds that are a mixture of R
656 and S forms. The results of the densitometric analysis are shown on the right as graphs. The
657 expression level of each protein in the control group (DMSO) is designated as 1. (actin levels
658 were used as loading control). All the compounds suppressed Caspase-3 cleavage without major
659 changes in the expression levels of Bax, Bcl-2, and Bcl-XL. The result of the t-test statistical
660 analysis is shown in each graph. “ns”: No statistically significant difference was detected
661 ($p>0.05$).
662
663

664 **Figure 2 Hit-to-Lead optimization of the novel cytoprotective small molecules (CSMs).**

665

666 A: Chemical structures of newly designed and synthesized lead compounds. The most effective
667 cell death inhibitor in cell culture, M41S, was developed based on the common chemical
668 structure of M5S and M6S (Series 1). The orally bioactive CSM, M109S, was developed from
669 M41S. M11 was the most effective cell death inhibitor among the inhibitors designed from M7
670 (Series 2).

671

672 B-D: Caspase activity of iBax cells treated with CSMs. Bax-mediated apoptosis was induced by
673 Dox addition to the culture medium in iBax cells in the presence of various concentrations of
674 CSMs as indicated in the graphs. The improvement of apoptosis inhibition through Hit-to-Lead
675 optimization is shown in B (M41S vs M5S and M5R) and C (M11 vs M7). D shows the
676 comparison of M41S (the best cell death inhibitor in cell culture), M109S (orally bioavailable
677 CSM designed from M41S), and Elthrmpag (previously reported Bax inhibitor).

678

679 E-G: Pharmacokinetic analysis of M109S in rodents. M109S was administered to mice and rats
680 by intraperitoneal injection (IP, 1 mg/kg), intravenous injection (IV, 5 mg/kg), or oral gavage
681 (PO, 10 mg/kg). The concentration of M109S was measured by Mass Spectrometry analysis. G:
682 M109S concentrations in the blood, brain, and retina 24 h after the administration (oral gavage
683 (PO) or intravenous injection (IV)) in rats.

684

685

686

687

688 **Figure 3 M109S protects the retina from bright light-induced injury in *Abc4$^{-/-}$Rdh8$^{-/-}$* mice**
689 **and Balb/cJ mice.**
690

691 A and B: A, The *in vivo* whole fundus imaging from *Abca4$^{-/-}$Rdh8$^{-/-}$* mice taken with scanning laser
692 ophthalmoscopy (SLO) one week after exposure to bright light. Autofluorescence spots (AF)
693 representing macrophages and microglial cells activated by light injury to clear dying
694 photoreceptors were detected in only vehicle-treated mice, but not in M109S-treated mice (10
695 mg/kg/b.w.). Scale bar, 1 mm. B, Quantification of the AF. M109s at 10 mg/kg/b.w showed
696 statistically significant protection against light-induced photoreceptor cell death. Statistical
697 analysis was performed with the two-way ANOVA and post hoc Turkey tests. The values of
698 $p<0.05$ were considered statistically significant. No statistically significant changes were labeled
699 as "ns".

700 C and D: C, The Spectral Domain Optical Coherence Tomography (SD-OCT) images of the
701 retina from *Abca4$^{-/-}$Rdh8$^{-/-}$* mice taken one week after illumination. Scale bar, 100 µm. D, The
702 measurement and statistical analysis of the ONL thickness in SD-OCT images. The exposure to
703 bright light-induced the degeneration of photoreceptors, which caused the shortening of the outer
704 nuclear layer (ONL) in retinas in vehicle-treated control mice, but not in the M109S-treated
705 group. M109S showed a dose-dependent effect protecting the photoreceptor cells from light-
706 induced death. Statistical analysis was performed with the two-way ANOVA and post hoc
707 Turkey tests. The values of $p<0.05$ were considered statistically significant. No statistically
708 significant changes were labeled as "ns".

709 E, The hematoxylin and eosin (H&E) staining of the retina sections of *Abca4$^{-/-}$Rdh8$^{-/-}$* mice.
710 M109S treatment mitigated degenerative processes in the retina. The thickness of the ONL in

711 mice treated with M109S at 10 mg/kg b.w. closely resembled the thickness of the retina in dark-
712 adapted mice. Scale bar, 50 µm.

713 F, Immunohistochemical analysis of the retina of *Abca4*$^{-/-}$*Rdh8*$^{-/-}$ mice. The cryosections were
714 stained with an anti-rhodopsin antibody recognizing the C-terminus (1D4 antibody) to detect rod
715 photoreceptors (red) and with peanut agglutinin to detect cone photoreceptors (green). Nuclei
716 were stained with DAPI (blue). M109S treatment prevented the degeneration of both rod and
717 cone photoreceptors. Scale bar, 50 µm.

718 G and H: The measurement and statistical analysis of the thickness of the ONL in the H&E-
719 stained sections of the retina of *Abca4*$^{-/-}$*Rdh8*$^{-/-}$ mice (G) and Balb/cJ mice (H). The treatment
720 with M109S (10 mg/kg/b.w.) treatment prevented the thickening of the ONL caused by the
721 bright light injury in both mouse strains.

722

723

724

725 **Figure 4 Effects of M109S on drug-induced apoptosis in cell culture**

726

727 A-C: M109S suppressed apoptosis induced by ABT-737 wild type (A), Bax only (*bax*$^{+/+}$*bak*$^{-/-}$)
728 (B), and Bak only (*bax*$^{-/-}$*bak*$^{+/+}$) (C) MEFs. MEFs were cultured with ABT-737 (1 μM) with
729 various doses of M109S for 24 h (WT and Bax only) or 48 h (Bak only). Caspase activitiy of
730 vehicle control (ABT-737 and vehicle) was designated as 100%.

731

732 D: M109S suppressed staurosporine (STS)-induced apoptosis in MEFs. MEFs were treated with
733 STS (1 μM) for 4 h in the presence of various concentrations as indicated in the graph. M109S
734 suppressed STS-induced caspase activation in a -dose-dependent manner. The result of the
735 Student's t-test statistical analysis is shown in each graph. "ns": No statistically significant
736 difference was detected ($p>0.05$).

737

738 E: M109S inhibited etoposide-induced apoptosis in Neuro2a cells. Neuro2a cells were treated
739 with etoposide (12.5 μM) for 24 h. Then, the medium was changed, and cells were incubated
740 with various concentrations of M109S for an additional 24 h without etoposide. M109S
741 suppressed etoposide-induced caspase activation. The result of the Student's t-test statistical
742 analysis is shown in each graph. "ns": No statistically significant difference was detected
743 ($p>0.05$).

744

745 F: M109S was not able to inhibit etoposide-induced apoptosis in HeLa cells. HeLa cells were
746 treated with Etoposide (12.5 μM) for 24 hrs. Then, the medium was changed, and cells were
747 incubated with various concentrations of M109S for an additional 24 h without Etoposide.

748 M109S did not show significant inhibition of Etoposide-induced caspase activation in HeLa
749 cells. The graph shows the results of 12.5 μM Etoposide. The result of the Student's t-test
750 statistical analysis is shown in each graph. "ns": No statistically significant difference was
751 detected ($p>0.05$).
752
753 G-I: M109S inhibited Obatoclax-induced apoptosis in ARPE19 cells. AREP19 cells were
754 incubated with Obatoclax (100 nM) in the presence of 500 nM CSMs (M41S, M11, and M109S)
755 for 24 h. Then, cells were collected and Western analyses of Caspase-3 and Bax were performed.
756 CSMs suppressed obatoclax-induced Caspase activation (p18 fragment production by the
757 cleavage of Caspase-3) (G). Bax expression was not affected by CSMs (I) (actin levels were used
758 as loading control). The result of the Student's t-test analysis is shown in each graph. "ns": No
759 statistically significant difference was detected ($p>0.05$).
760
761
762
763
764
765
766
767

768 **Figure 5. M109S inhibits Bax activation.**

769

770 A and B: CSMs suppressed conformation change of Bax. The N-terminus exposure of Bax
771 occurs at the early step of Bax activation. Activated (conformationally changed) Bax can be
772 immunoprecipitated by the 6A7 monoclonal antibody recognizing the N-terminus of Bax. iBax
773 cells were treated with Dox for 48 hrs in the presence or absence of CSMs (M41S (50nM),
774 M109S (500nM), or M11 (500nM)). Cells were lysed with CHAPS buffer and the lysates were
775 subjected to immunoprecipitation (ip). C: Western blot of immunoprecipitated Bax by 6A7
776 antibody and total Bax in the cell lysates are shown. D: The ratio of the Western blot intensity of
777 immunoprecipitated Bax (IP) and total Bax (total) is shown. CSMs significantly suppressed the
778 amount of immunoprecipitated Bax without a significant change in the total Bax expression. The
779 result of the Student's t-test statistical analysis is shown in each graph. "ns": No statistically
780 significant difference was detected ($p>0.05$).

781

782 C and D: CSMs suppressed mitochondrial translocation of Bax. iBax cells were fixed at 36 h
783 after Dox treatment. Bax was detected by an anti-Bax polyclonal antibody (green fluorescence).
784 The activation of the Dox-inducible promoter was confirmed by the detection of mCherry by red
785 fluorescence. In vehicle (DMSO) control, punctuated Bax staining patterns associated with
786 mitochondrial translocation were detected (indicated by arrows). The frequency of the
787 punctuated staining was significantly reduced by CSMs (M41S, M11, and M109S). D:
788 Quantitative analysis of Fig.5C is shown. The result of the Students' t-test statistical analysis is
789 shown in graph (B). "ns": No statistically significant difference was detected ($p>0.05$).

790

791 E and F: CSMs bind purified recombinant Bax proteins. The interactions of CSMs and Bax were
792 examined by microscale thermal shift (MST) assay using His-tagged Bax. Panel E shows a
793 representative dose-dependent Bax binding signal curve of M109S. A similar binding assay was
794 performed multiple times, and the average of Kd was 153.75+55.8 nM (n=4). Panel F shows a
795 negative control experiment. The binding of Bax and Dexamethasone was not detected.
796
797
798
799
800
801

802 **Figure 6. Effects of M109s on cellular metabolism**

803

804 A-H: M109S decreased the maximum oxygen consumption rate (OCR) and increased the
805 extracellular acidification rate (ECAR) both in *wt* and *bax*$^{-/-}$*bak*$^{-/-}$ MEFs. OCR and ECAR
806 represent the activities of mitochondrial oxidative phosphorylation (OXPHOS) and glycolysis,
807 respectively. The effect of M109S on metabolism was analyzed using the Seahorse mitochondria
808 stress kit as described in Method section. MEFs (*wt* and *bax*$^{-/-}$*bak*$^{-/-}$) were incubated with or
809 without M109s for 4 h before Seahorse analysis. M109S was also added to the culture medium
810 during the Seahorse analysis procedure (approximately 3 h). A-F: The levels of OCR of the basal
811 (A, B), ATP production (C, D), and maximum oxygen consumption (E, F), are shown. G and H:
812 The basal ECAR is shown. M109S decreased maximal O_2 consumption and increased glycolysis
813 in *wt* and *bax*$^{-/-}$*bak*$^{-/-}$ MEFs. The result of the Student's t-test statistical analysis is shown in each
814 graph. "ns": No statistically significant difference was detected ($p>0.05$).

815

816

817 I and J: M109S decreases ROS levels in cell culture. ROS levels were measured by ROS-Glo-
818 H_2O_2 assay kit (Promega). N-acetyl cysteine (NAC) or M109S was added to the culture medium
819 for a total of 8 h (4 hrs before ROS substrate addition and 4 h during the incubation with ROS
820 substrate). M109S addition decreased ROS levels both in *wt* and *bax*$^{-/-}$*bak*$^{-/-}$ MEFs. The result of
821 Studen's t-test statistical analysis is shown in each graph. "ns": No statistically significant
822 difference was detected ($p>0.05$).

823

824 K and L: A high dose of M109S (1 μM) slowed the cell division speed both in *wt* and *bax*$^{-/-}$*bak*$^{-/-}$
825 MEFs. Forty thousand cells were plated in each well of 12 well plate (1 ml/well) on Day 0. The
826 next day (24 h later), M109S was added to the medium, and cells were cultured for an additional
827 24 h, and the numbers of cells were counted. The cell number at Day 0 is designated 100%, and
828 the ratio of cell number is shown. The result of the Student's t-test statistical analysis is shown in
829 each graph. "ns": No statistically significant difference was detected ($p>0.05$).
830
831 M: Schematic explanation of the mechanism of action of CSMs.
832
833
834
835
836
837
838

839 **Supplemental Figure S1**

840 The effect of M109S concentration on retina inflammation was examined *in vivo* in the whole
841 fundus images of *Abca4*$^{-/-}$*Rdh8*$^{-/-}$ mice taken with scanning laser ophthalmoscopy (SLO) one week
842 after exposure to bright light. Autofluorescence spots (AF) representing macrophages and
843 microglial cells activated by light injury to clear dying photoreceptors were detected in vehicle-
844 treated mice, but not in M109S-treated mice at 10 mg/kg/b.w. However, lower doses of M109S
845 were not effective. Scale bar, 1 mm.

846

847 **Supplemental Figure S2**

848 Concentration-dependent effect of M109S protecting against light-induced retina degeneration.
849 The Spectral Domain Optical Coherence Tomography (SD-OCT) images of the retina from
850 *Abca4*$^{-/-}$*Rdh8*$^{-/-}$ mice were taken one week after illumination. Scale bar, 100 µm. The exposure to
851 bright light-induced cell death of photoreceptors, which caused shortening of the outer nuclear
852 layer (ONL) in the retinas of vehicle-treated control mice. Retina degeneration was prevented by
853 M109S at 10 and 20 mg/kg/b.w. However, lower doses (1, 2.5, and 5 mg/kg) were not effective.

854

855 **Supplemental Figure S3**

856 M109S at 10 mg/kg b.w. protected photoreceptors of Balb/cJ mice from light-induced cell death.
857 As detected in the OCT images (A) and H&E stained the retina sections (B) the thickness of the
858 ONL layer resembled the one observed in dark-adapted control mice, while vehicle-treated mice
859 showed severe shortening of the ONL as a result of photoreceptor cells death. Scale bar in (A)
860 100 µm and in (B) 50 µm.

861

862 **Supplemental Figure S4**

863 M109S was not able to inhibit etoposide-induced apoptosis in HeLa cells. HeLa cells were
864 treated with etoposide (25 μM) for 24 h. Then, the medium was changed, and cells were
865 incubated with various concentrations of M109S for an additional 24 h without etoposide.
866 M109S did not show a significant inhibition of etoposide-induced caspase activation in HeLa
867 cells, except for a slight inhibition at 125 nM. The result of the Student's t-test statistical analysis
868 is shown in each graph. "ns": No statistically significant difference was detected ($p>0.05$).

869

870 **Supplemental Figure S5**

871 Microscale thermal shift (MST) assay detecting the binding of CSMs and Bax.
872 A: The binding of Bax and M41S was detected when the interaction was determined using 1%
873 NP40-containing buffer. B: The binding of Bax and M41S was not detected in 1% Chaps buffer.

874

875

Reference

Amgalan, D., Garner, T.P., Pekson, R., Jia, X.F., Yanamandala, M., Paulino, V., Liang, F.G., Corbalan, J.J., Lee, J., Chen, Y., et al. (2020). A small-molecule allosteric inhibitor of BAX protects against doxorubicin-induced cardiomyopathy. Nat Cancer *1*, 315-328. 10.1038/s43018-020-0039-1.

Amsterdam, A., Tajima, K., and Sasson, R. (2002). Cell-specific regulation of apoptosis by glucocorticoids: implication to their anti-inflammatory action. Biochem Pharmacol *64*, 843-850. 10.1016/s0006-2952(02)01147-4.

Ashkenazi, A., Fairbrother, W.J., Leverson, J.D., and Souers, A.J. (2017). From basic apoptosis discoveries to advanced selective BCL-2 family inhibitors. Nat Rev Drug Discov *16*, 273-284. 10.1038/nrd.2016.253.

Bombrun, A., Gerber, P., Casi, G., Terradillos, O., Antonsson, B., and Halazy, S. (2003). 3,6-dibromocarbazole piperazine derivatives of 2-propanol as first inhibitors of cytochrome c release via Bax channel modulation. Journal of medicinal chemistry *46*, 4365-4368. 10.1021/jm034107j.

Certo, M., Del Gaizo Moore, V., Nishino, M., Wei, G., Korsmeyer, S., Armstrong, S.A., and Letai, A. (2006). Mitochondria primed by death signals determine cellular addiction to antiapoptotic BCL-2 family members. Cancer cell *9*, 351-365. 10.1016/j.ccr.2006.03.027.

Chen, Y., Okano, K., Maeda, T., Chauhan, V., Golczak, M., Maeda, A., and Palczewski, K. (2012). Mechanism of all-trans-retinal toxicity with implications for stargardt disease and age-related macular degeneration. The Journal of biological chemistry *287*, 5059-5069. 10.1074/jbc.M111.315432.

Cunnane, S.C., Trushina, E., Morland, C., Prigione, A., Casadesus, G., Andrews, Z.B., Beal, M.F., Bergersen, L.H., Brinton, R.D., de la Monte, S., et al. (2020). Brain energy rescue: an emerging therapeutic concept for neurodegenerative disorders of ageing. Nat Rev Drug Discov *19*, 609-633. 10.1038/s41573-020-0072-x.

Diepstraten, S.T., Anderson, M.A., Czabotar, P.E., Lessene, G., Strasser, A., and Kelly, G.L. (2022). The manipulation of apoptosis for cancer therapy using BH3-mimetic drugs. Nat Rev Cancer *22*, 45-64. 10.1038/s41568-021-00407-4.

Edlich, F., Banerjee, S., Suzuki, M., Cleland, M.M., Arnoult, D., Wang, C., Neutzner, A., Tjandra, N., and Youle, R.J. (2011). Bcl-x(L) retrotranslocates Bax from the mitochondria into the cytosol. Cell *145*, 104-116. 10.1016/j.cell.2011.02.034.

Ezerina, D., Takano, Y., Hanaoka, K., Urano, Y., and Dick, T.P. (2018). N-Acetyl Cysteine Functions as a Fast-Acting Antioxidant by Triggering Intracellular H2S and Sulfane Sulfur Production. Cell chemical biology *25*, 447-459 e444. 10.1016/j.chembiol.2018.01.011.

920 Gama, V., Gomez, J.A., Mayo, L.D., Jackson, M.W., Danielpour, D., Song, K., Haas, A.L.,
921 Laughlin, M.J., and Matsuyama, S. (2009). Hdm2 is a ubiquitin ligase of Ku70-Akt promotes
922 cell survival by inhibiting Hdm2-dependent Ku70 destabilization. Cell death and differentiation
923 *16*, 758-769. 10.1038/cdd.2009.6.
924
925 Gao, H., Tripathi, U., Trushin, S., Okromelidze, L., Pichurin, N.P., Wei, L., Zhuang, Y., Wang,
926 L., and Trushina, E. (2021). A genome-wide association study in human lymphoblastoid cells
927 supports safety of mitochondrial complex I inhibitor. Mitochondrion *58*, 83-94.
928 10.1016/j.mito.2021.02.005.
929
930 Gao, S., Parmar, T., Palczewska, G., Dong, Z., Golczak, M., Palczewski, K., and Jastrzebska, B.
931 (2018). Protective Effect of a Locked Retinal Chromophore Analog against Light-Induced
932 Retinal Degeneration. Mol Pharmacol *94*, 1132-1144. 10.1124/mol.118.112581.
933 Garner, T.P., Amgalan, D., Reyna, D.E., Li, S., Kitsis, R.N., and Gavathiotis, E. (2019). Small-
934 molecule allosteric inhibitors of BAX. Nature chemical biology *15*, 322-330. 10.1038/s41589-
935 018-0223-0.
936
937 Gascoyne, D.M., Kypta, R.M., and Vivanco, M. (2003). Glucocorticoids inhibit apoptosis during
938 fibrosarcoma development by transcriptionally activating Bcl-xL. The Journal of biological
939 chemistry *278*, 18022-18029. 10.1074/jbc.M301812200.
940
941 Gohil, V.M., Sheth, S.A., Nilsson, R., Wojtovich, A.P., Lee, J.H., Perocchi, F., Chen, W., Clish,
942 C.B., Ayata, C., Brookes, P.S., and Mootha, V.K. (2010). Nutrient-sensitized screening for drugs
943 that shift energy metabolism from mitochondrial respiration to glycolysis. Nat Biotechnol *28*,
944 249-255. 10.1038/nbt.1606.
945
946 Grover, G.J., and Malm, J. (2008). Pharmacological profile of the selective mitochondrial F1F0
947 ATP hydrolase inhibitor BMS-199264 in myocardial ischemia. Cardiovasc Ther *26*, 287-296.
948 10.1111/j.1755-5922.2008.00065.x.
949
950 Han, Y., Qu, Y.Q., Mok, S.W.F., Chen, J., Xia, C.L., He, H.Q., Li, Z., Zhang, W., Qiu, C.L., Liu,
951 L., et al. (2019). A Novel Drug Resistance Mechanism: Genetic Loss of Xeroderma
952 Pigmentosum Complementation Group C (XPC) Enhances Glycolysis-Mediated Drug
953 Resistance in DLD-1 Colon Cancer Cells. Front Pharmacol *10*, 912. 10.3389/fphar.2019.00912.
954 Hong, S., and Pedersen, P.L. (2008). ATP synthase and the actions of inhibitors utilized to study
955 its roles in human health, disease, and other scientific areas. Microbiol Mol Biol Rev *72*, 590-
956 641, Table of Contents. 10.1128/MMBR.00016-08.
957
958 Hsu, Y.T., and Youle, R.J. (1998). Bax in murine thymus is a soluble monomeric protein that
959 displays differential detergent-induced conformations. The Journal of biological chemistry *273*,
960 10777-10783.
961
962 Jensen, K., WuWong, D.J., Wong, S., Matsuyama, M., and Matsuyama, S. (2019).
963 Pharmacological inhibition of Bax-induced cell death: Bax-inhibiting peptides and small
964 compounds inhibiting Bax. Experimental biology and medicine *244*, 621-629.
965 10.1177/1535370219833624.

Johnson, J.A., and Ogbi, M. (2011). Targeting the F1Fo ATP Synthase: modulation of the body's powerhouse and its implications for human disease. Curr Med Chem *18*, 4684-4714. 10.2174/092986711797379177.

Kim, S.R., Fishkin, N., Kong, J., Nakanishi, K., Allikmets, R., and Sparrow, J.R. (2004). Rpe65 Leu450Met variant is associated with reduced levels of the retinal pigment epithelium lipofuscin fluorophores A2E and iso-A2E. Proceedings of the National Academy of Sciences of the United States of America *101*, 11668-11672. 10.1073/pnas.0403499101.

Loew, R., Heinz, N., Hampf, M., Bujard, H., and Gossen, M. (2010). Improved Tet-responsive promoters with minimized background expression. BMC Biotechnol *10*, 81. 10.1186/1472-6750-10-81.

Maeda, A., Maeda, T., Golczak, M., Chou, S., Desai, A., Hoppel, C.L., Matsuyama, S., and Palczewski, K. (2009). Involvement of all-trans-retinal in acute light-induced retinopathy of mice. The Journal of biological chemistry *284*, 15173-15183. 10.1074/jbc.M900322200.
Maeda, A., Maeda, T., Golczak, M., and Palczewski, K. (2008). Retinopathy in mice induced by disrupted all-trans-retinal clearance. The Journal of biological chemistry *283*, 26684-26693. 10.1074/jbc.M804505200.

Matsuyama, S., Greenlee, W. (2020). The use of novel small compounds of Bax inhibitors to protect damaged cells from death. US Patent Office, https://patents.google.com/patent/WO2021002986A2/en.

Matsuyama, S., Xu, Q., Velours, J., and Reed, J.C. (1998). The Mitochondrial F0F1-ATPase proton pump is required for function of the proapoptotic protein Bax in yeast and mammalian cells. Molecular cell *1*, 327-336.

Morciano, G., Preti, D., Pedriali, G., Aquila, G., Missiroli, S., Fantinati, A., Caroccia, N., Pacifico, S., Bonora, M., Talarico, A., et al. (2018). Discovery of Novel 1,3,8-Triazaspiro[4.5]decane Derivatives That Target the c Subunit of F1/FO-Adenosine Triphosphate (ATP) Synthase for the Treatment of Reperfusion Damage in Myocardial Infarction. Journal of medicinal chemistry *61*, 7131-7143. 10.1021/acs.jmedchem.8b00278.

Nechushtan, A., Smith, C.L., Hsu, Y.T., and Youle, R.J. (1999). Conformation of the Bax C-terminus regulates subcellular location and cell death. Embo J *18*, 2330-2341.

Niu, X., Brahmbhatt, H., Mergenthaler, P., Zhang, Z., Sang, J., Daude, M., Ehlert, F.G.R., Diederich, W.E., Wong, E., Zhu, W., et al. (2017). A Small-Molecule Inhibitor of Bax and Bak Oligomerization Prevents Genotoxic Cell Death and Promotes Neuroprotection. Cell chemical biology *24*, 493-506 e495. 10.1016/j.chembiol.2017.03.011.

Oltersdorf, T., Elmore, S.W., Shoemaker, A.R., Armstrong, R.C., Augeri, D.J., Belli, B.A., Bruncko, M., Deckwerth, T.L., Dinges, J., Hajduk, P.J., et al. (2005). An inhibitor of Bcl-2 family proteins induces regression of solid tumours. Nature *435*, 677-681. 10.1038/nature03579.

1011 Ortega, J.T., Parmar, T., Golczak, M., and Jastrzebska, B. (2021). Protective Effects of
1012 Flavonoids in Acute Models of Light-Induced Retinal Degeneration. Mol Pharmacol *99*, 60-77.
1013 10.1124/molpharm.120.000072.
1014
1015 Peixoto, P.M., Ryu, S.Y., Bombrun, A., Antonsson, B., and Kinnally, K.W. (2009). MAC
1016 inhibitors suppress mitochondrial apoptosis. The Biochemical journal *423*, 381-387.
1017 10.1042/BJ20090664.
1018
1019 Pogmore, J.P., Uehling, D., and Andrews, D.W. (2021). Pharmacological Targeting of
1020 Executioner Proteins: Controlling Life and Death. Journal of medicinal chemistry *64*, 5276-5290.
1021 10.1021/acs.jmedchem.0c02200.
1022
1023 Procaccio, V., Bris, C., Chao de la Barca, J.M., Oca, F., Chevrollier, A., Amati-Bonneau, P.,
1024 Bonneau, D., and Reynier, P. (2014). Perspectives of drug-based neuroprotection targeting
1025 mitochondria. Rev Neurol (Paris) *170*, 390-400. 10.1016/j.neurol.2014.03.005.
1026
1027 Sawada, O., Perusek, L., Kohno, H., Howell, S.J., Maeda, A., Matsuyama, S., and Maeda, T.
1028 (2014). All-trans-retinal induces Bax activation via DNA damage to mediate retinal cell
1029 apoptosis. Experimental eye research *123*, 27-36. 10.1016/j.exer.2014.04.003.
1030
1031 Singh, R., Letai, A., and Sarosiek, K. (2019). Regulation of apoptosis in health and disease: the
1032 balancing act of BCL-2 family proteins. Nature reviews. Molecular cell biology *20*, 175-193.
1033 10.1038/s41580-018-0089-8.
1034
1035 Spitz, A.Z., and Gavathiotis, E. (2022). Physiological and pharmacological modulation of BAX.
1036 Trends in pharmacological sciences *43*, 206-220. 10.1016/j.tips.2021.11.001.
1037
1038 Spitz, A.Z., Zacharioudakis, E., Reyna, D.E., Garner, T.P., and Gavathiotis, E. (2021).
1039 Eltrombopag directly inhibits BAX and prevents cell death. Nature communications *12*, 1134.
1040 10.1038/s41467-021-21224-1.
1041
1042 Stojakovic, A., Trushin, S., Sheu, A., Khalili, L., Chang, S.Y., Li, X., Christensen, T., Salisbury,
1043 J.L., Geroux, R.E., Gateno, B., et al. (2021). Partial inhibition of mitochondrial complex I
1044 ameliorates Alzheimer's disease pathology and cognition in APP/PS1 female mice. Commun
1045 Biol *4*, 61. 10.1038/s42003-020-01584-y.
1046
1047 Todt, F., Cakir, Z., Reichenbach, F., Youle, R.J., and Edlich, F. (2013). The C-terminal helix of
1048 Bcl-x(L) mediates Bax retrotranslocation from the mitochondria. Cell death and differentiation
1049 *20*, 333-342. 10.1038/cdd.2012.131.
1050
1051 Tu, H.C., Ren, D., Wang, G.X., Chen, D.Y., Westergard, T.D., Kim, H., Sasagawa, S., Hsieh,
1052 J.J., and Cheng, E.H. (2009). The p53-cathepsin axis cooperates with ROS to activate
1053 programmed necrotic death upon DNA damage. Proceedings of the National Academy of
1054 Sciences of the United States of America *106*, 1093-1098. 10.1073/pnas.0808173106.

1055 Vogler, M., Weber, K., Dinsdale, D., Schmitz, I., Schulze-Osthoff, K., Dyer, M.J., and Cohen,
1056 G.M. (2009). Different forms of cell death induced by putative BCL2 inhibitors. Cell death and
1057 differentiation *16*, 1030-1039. 10.1038/cdd.2009.48.
1058
1059 Walensky, L.D. (2019). Targeting BAX to drug death directly. Nature chemical biology *15*, 657-
1060 665. 10.1038/s41589-019-0306-6.
1061
1062 Wei, M.C., Zong, W.X., Cheng, E.H., Lindsten, T., Panoutsakopoulou, V., Ross, A.J., Roth,
1063 K.A., MacGregor, G.R., Thompson, C.B., and Korsmeyer, S.J. (2001). Proapoptotic BAX and
1064 BAK: a requisite gateway to mitochondrial dysfunction and death. Science *292*, 727-730.
1065 Wienken, C.J., Baaske, P., Rothbauer, U., Braun, D., and Duhr, S. (2010). Protein-binding assays
1066 in biological liquids using microscale thermophoresis. Nature communications *1*, 100.
1067 10.1038/ncomms1093.
1068

Fig.1

A

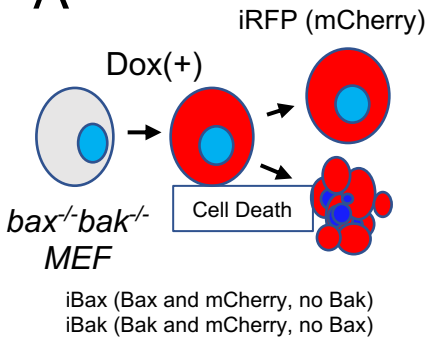

B

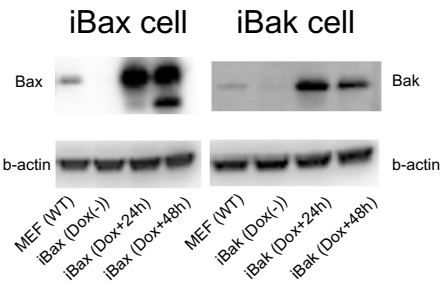

C

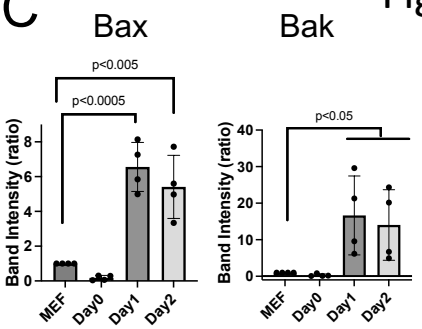

D

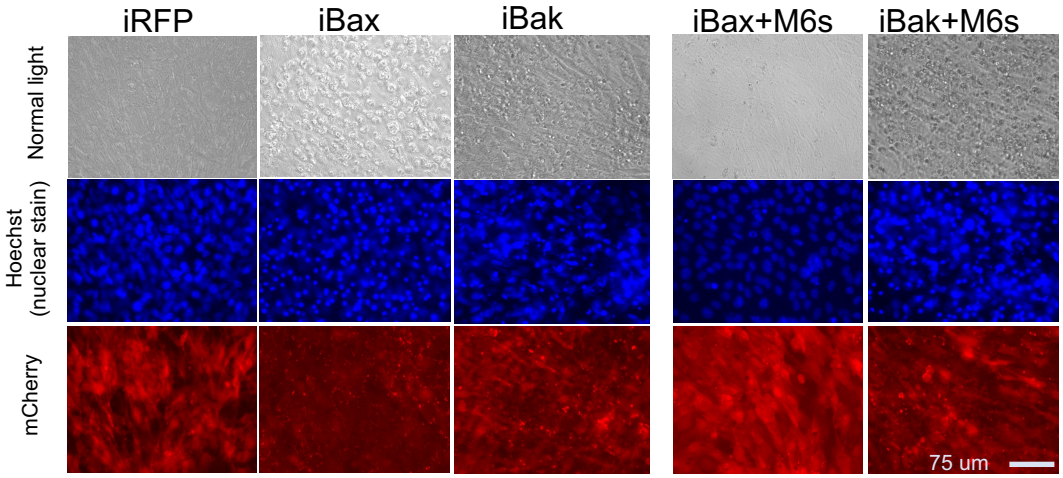

E

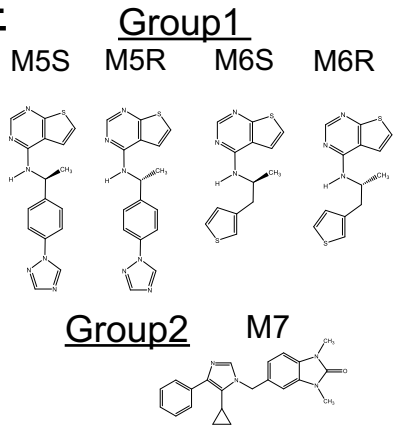

F

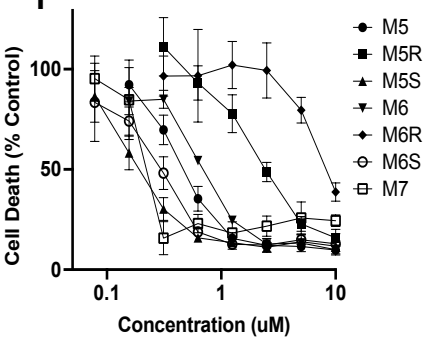

G

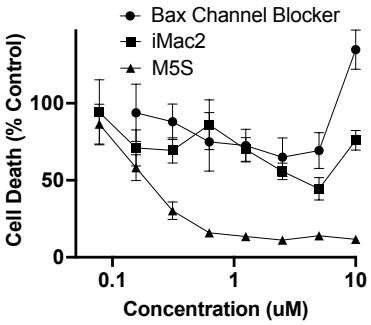

H

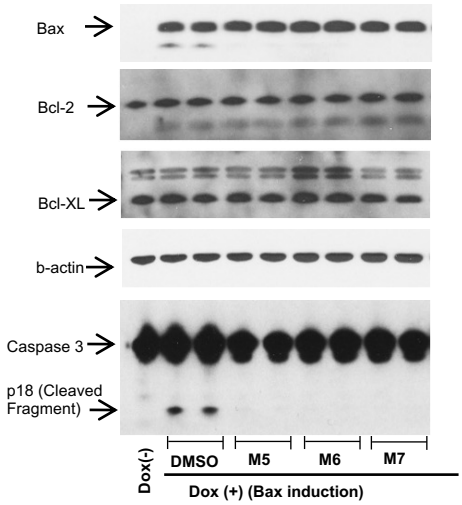

I

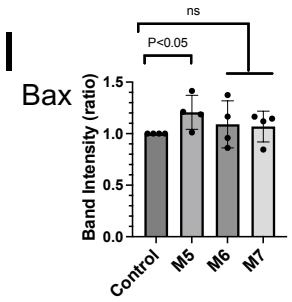

J

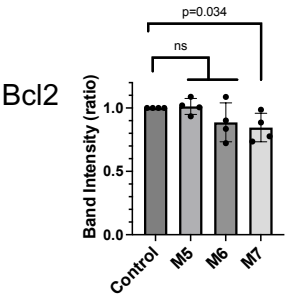

K

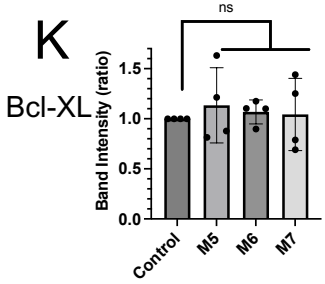

L

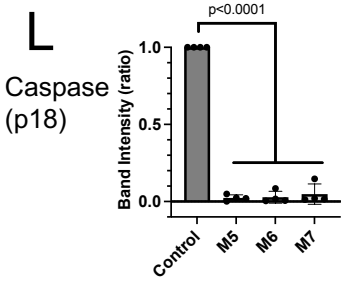

Fig.2

A

Series 1

M41S

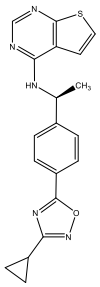

M109S

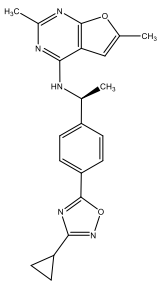

Series 2

M11

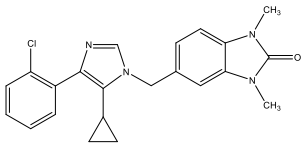

B

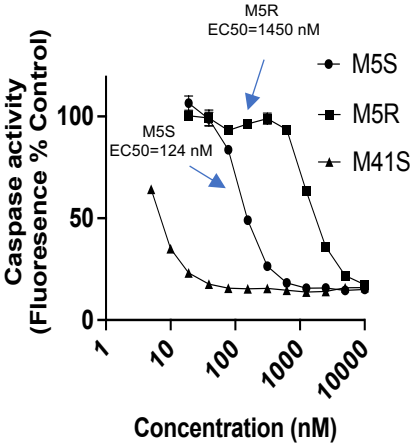

C

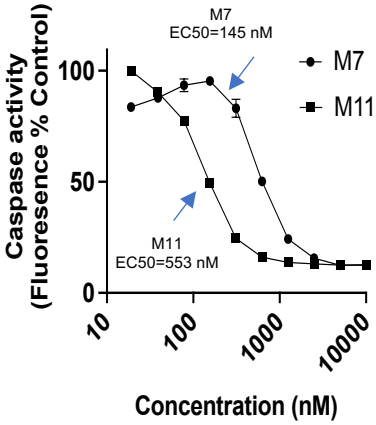

D

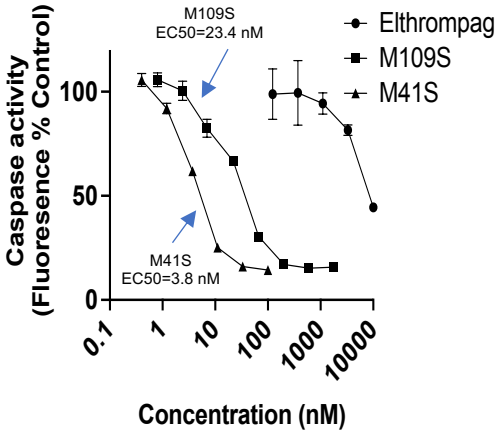

E

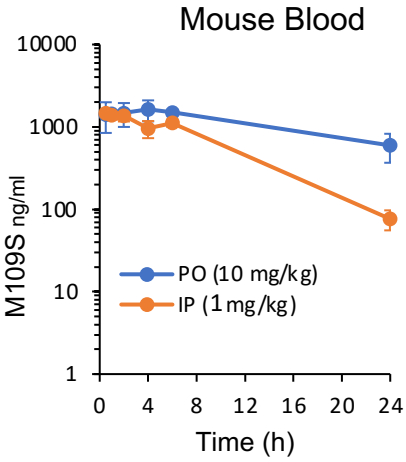

OP (10 mg/kg): $t_{1/2}$ **>12h**
IP (1mg/kg): $t_{1/2}$**=5.22h**

F

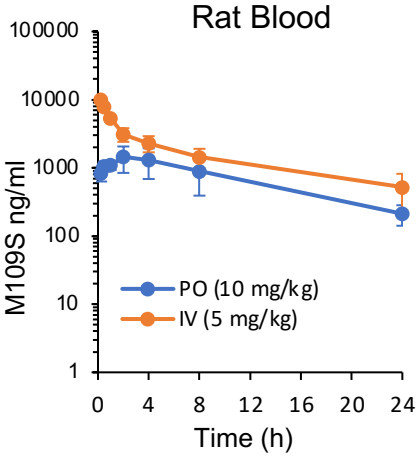

OP (10 mg/kg): $t_{1/2}$ **=9.7h**
IV (5mg/kg): $t_{1/2}$**=7.6h**

G

M109S concentration
24 h after administration (rat)

		Blood	Brain	Retina
PO (10mg/kg)	ng/ml	212±70.6	64.3±19.5	83.5±28
	nM	565.3±188.3	171±52	222.7±74.7

		Blood	Brain	Retina
IV (5 mg/kg)	ng/ml	522±295	190±74.2	229±132
	nM	1392±768.7	506.7±197.9	610±352

Fig.3

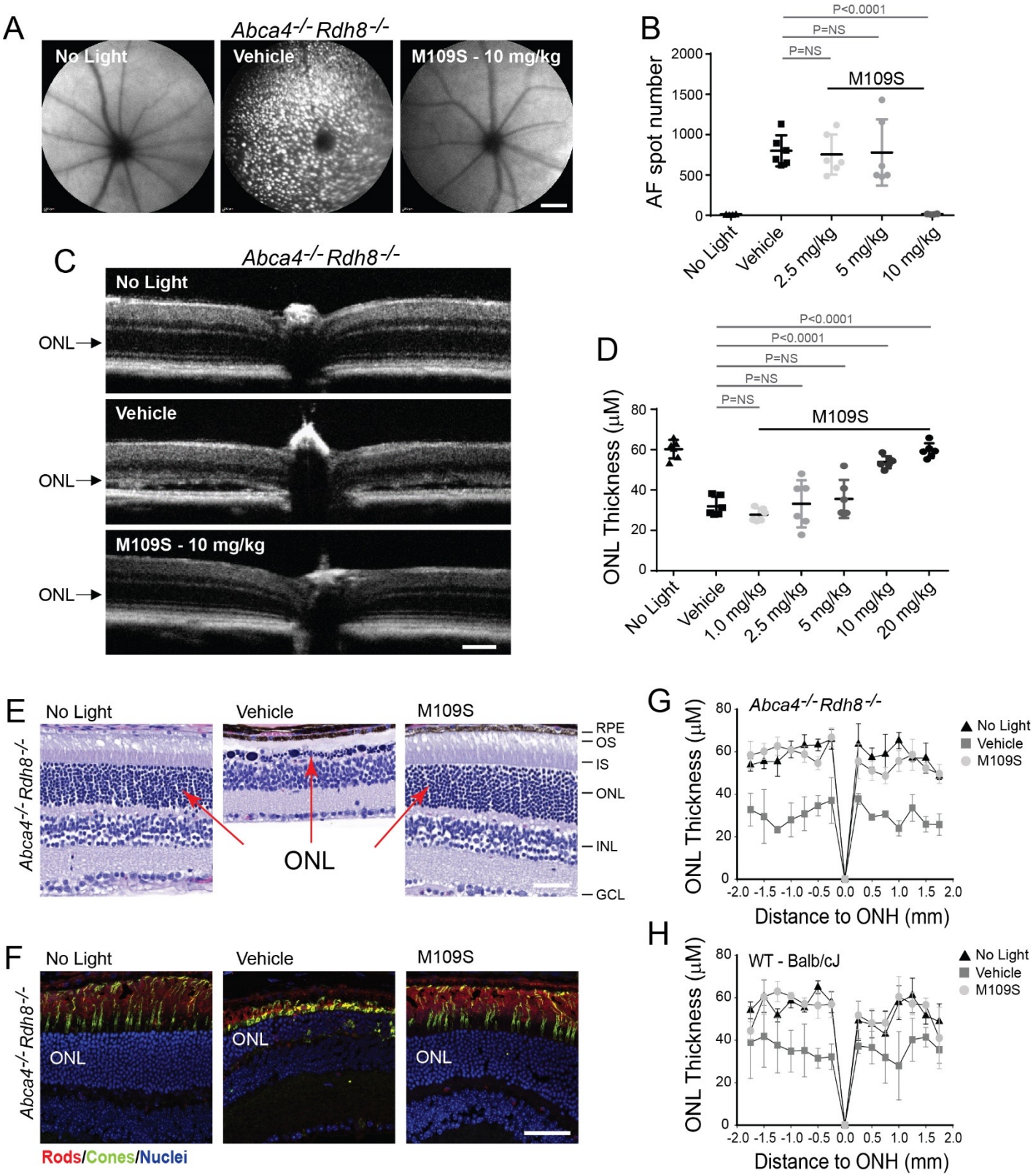
A
Abca4-/- Rdh8-/-
No Light
Vehicle
M109S - 10 mg/kg
B
P<0.0001
P=NS
P=NS
M109S
AF spot number
2000
1500
1000
500
0
No Light
Vehicle
2.5 mg/kg
5 mg/kg
10 mg/kg
C
Abca4-/- Rdh8-/-
No Light
ONL
Vehicle
ONL
M109S - 10 mg/kg
ONL
D
P<0.0001
P<0.0001
P=NS
P=NS
P=NS
M109S
ONL Thickness (μM)
80
60
40
20
0
No Light
Vehicle
1.0 mg/kg
2.5 mg/kg
5 mg/kg
10 mg/kg
20 mg/kg
E
No Light
Vehicle
M109S
Abca4-/- Rdh8-/-
RPE
OS
IS
ONL
INL
GCL
ONL
G
Abca4-/- Rdh8-/-
No Light
Vehicle
M109S
ONL Thickness (μM)
80
60
40
20
0
-2.0 -1.5 -1.0 -0.5 0.0 0.5 1.0 1.5 2.0
Distance to ONH (mm)
F
No Light
Vehicle
M109S
Abca4-/- Rdh8-/-
ONL
ONL
ONL
Rods/Cones/Nuclei
H
WT - Balb/cJ
No Light
Vehicle
M109S
ONL Thickness (μM)
80
60
40
20
0
-2.0 -1.5 -1.0 -0.5 0.0 0.5 1.0 1.5 2.0
Distance to ONH (mm)

Fig.4

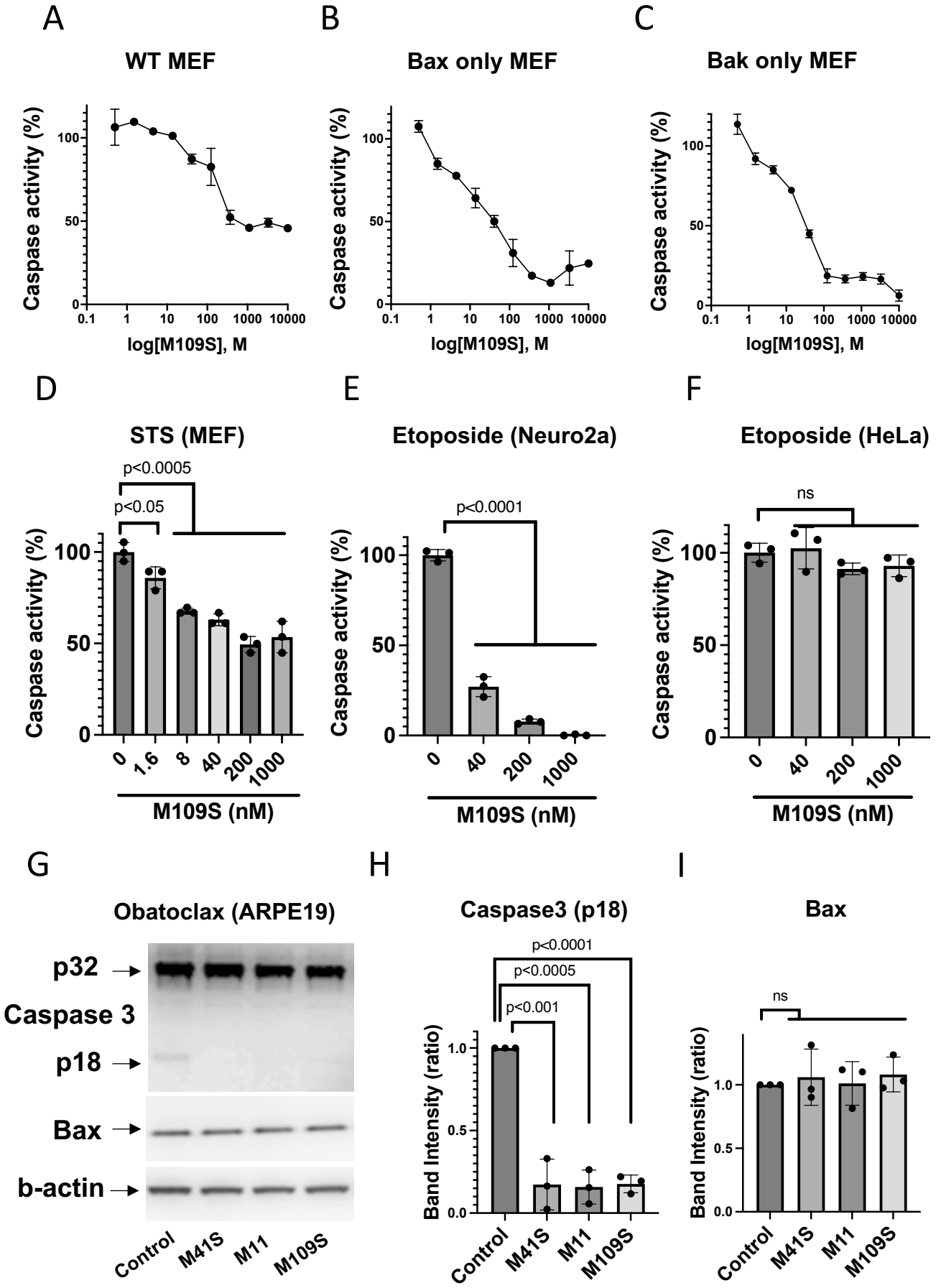
A
WT MEF
Caspase activity (%)
log[M109S], M
B
Bax only MEF
C
Bak only MEF
D
STS (MEF)
p<0.0005
p<0.05
M109S (nM)
E
Etoposide (Neuro2a)
p<0.0001
F
Etoposide (HeLa)
ns
G
Obatoclax (ARPE19)
p32
Caspase 3
p18
Bax
b-actin
Control
M41S
M11
M109S
H
Caspase3 (p18)
p<0.0001
p<0.0005
p<0.001
Band Intensity (ratio)
I
Bax

Fig.5

A

Active Bax immunoprecipitated by 6A7 ab

Bax in the cell lysate

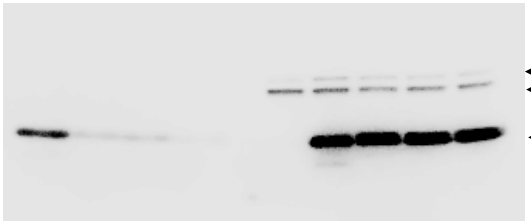

DMSO M41S M109S M11 Dox (-) DMSO M41S M109S M11

Dox(+) (Bax+) Dox(+) (Bax+)

B

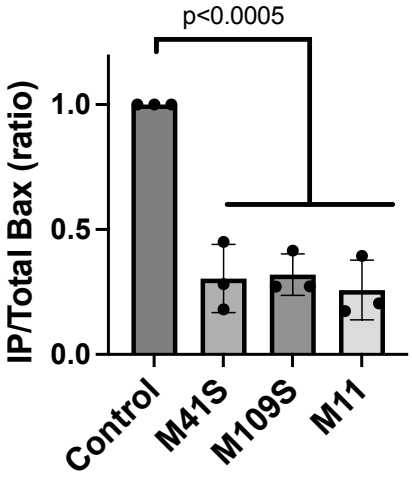

C

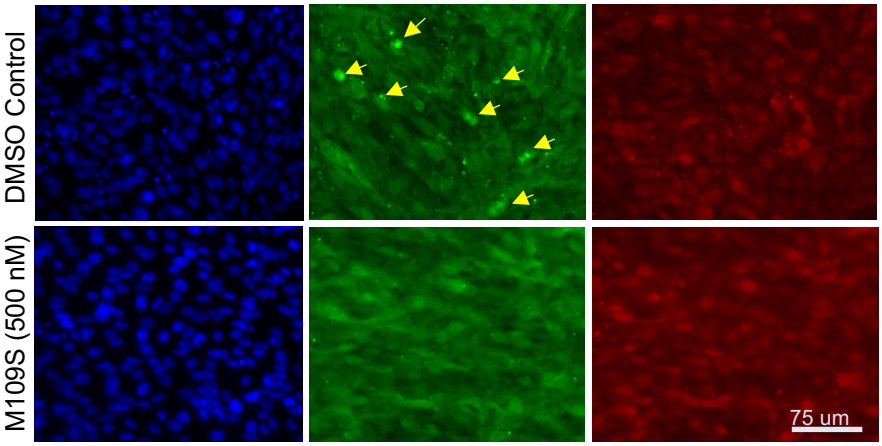

D

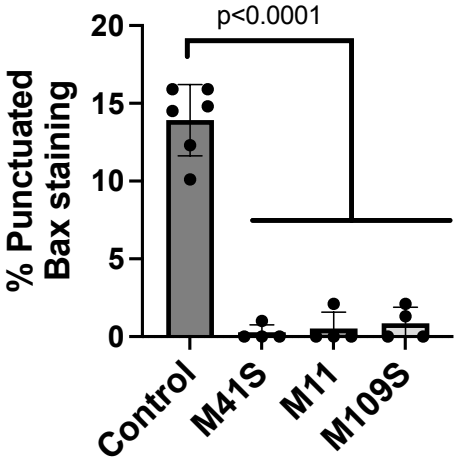

E

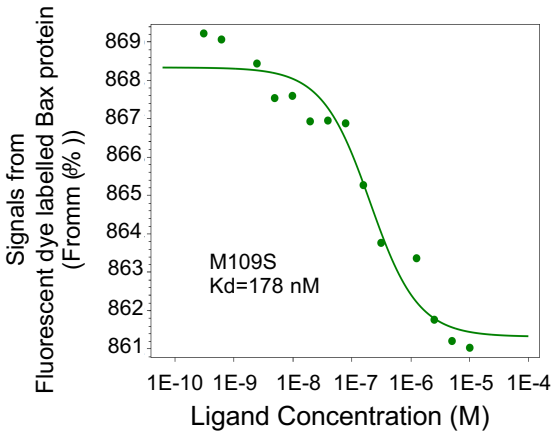

F

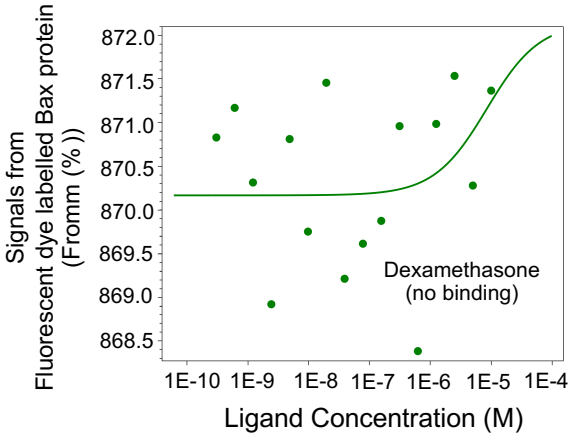

Fig.6

Basal O_2 Consumption

O_2 Consumption for ATP production

Maximal O_2 Consumption
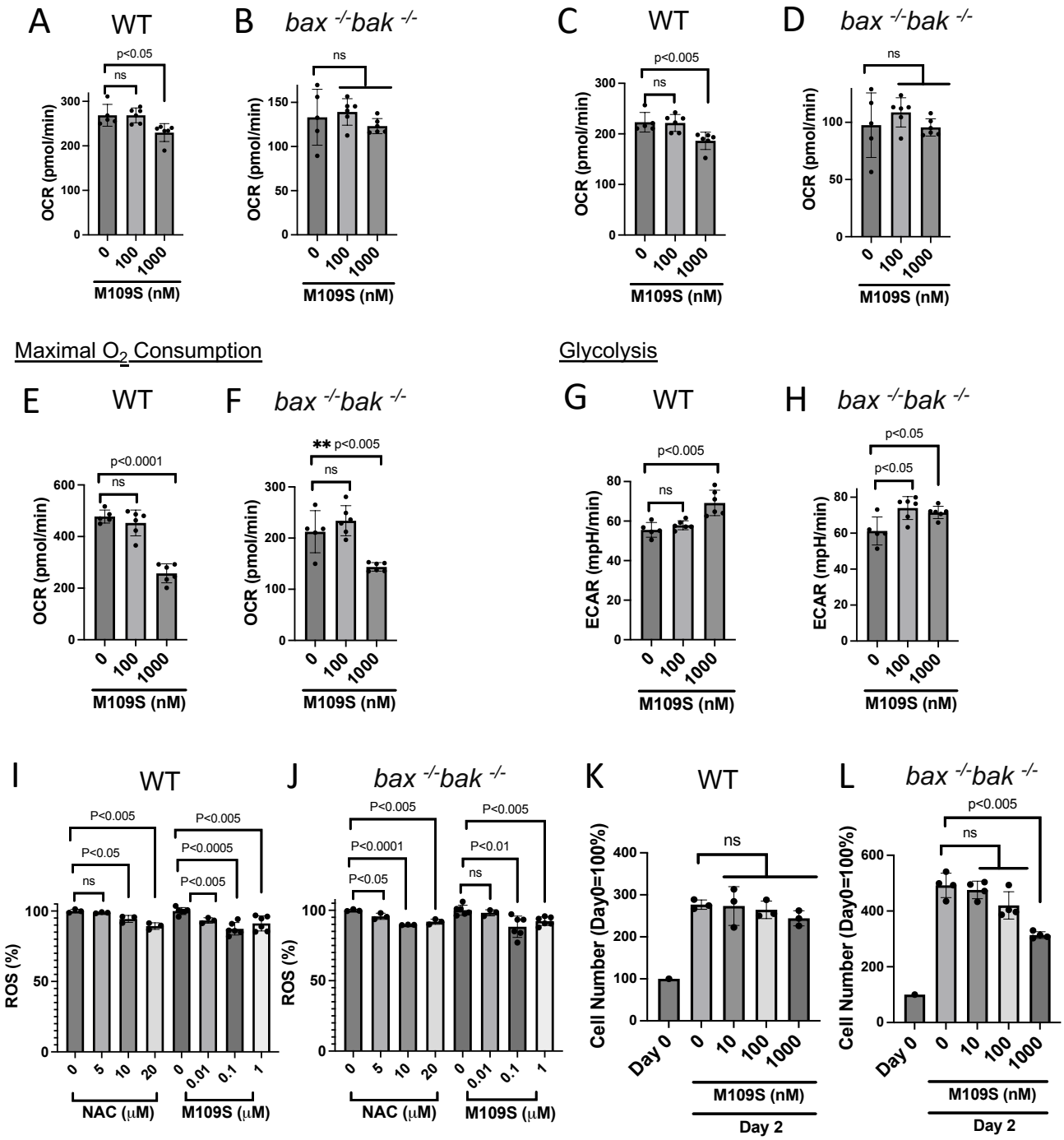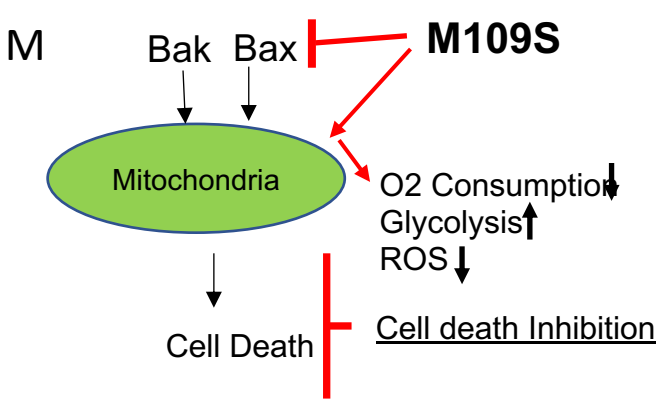
Glycolysis